SEDIMENTOLOGY the journal of the International Association of Sedimentologists

Sedimentology (2020) doi: 10.1111/sed.12792

Diagnostic criteria using microfacies for calcareous contourites, turbidites and pelagites in the Eocene–Miocene slope succession, southern Cyprus

HEIKO HÜNEKE*, F. JAVIER HERNÁNDEZ-MOLINA†, FRANCISCO J. RODRÍGUEZ-TOVAR‡, ESTEFANÍA LLAVE§, DOMENICO CHIARELLA†, ANXO MENA¶ and DORRIK A. V. STOW**

**Institut für Geographie und Geologie, Universität Greifswald, Jahn-Strasse 17a, 17487 Greifswald, Germany (E-mail: hueneke@uni-greifswald.de)*

†Department of Earth Sciences, Royal Holloway University of London, Egham, Surrey TW20 0EX, UK

‡Departamento de Estratigrafía y Paleontología, Universidad de Granada, 18002 Granada, Spain

§Instituto Geológico y Minero de España, 28003 Madrid, Spain

¶Departamento de Xeociencias Mariñas e Ordenación do Territorio, Universidad de Vigo, E-36310 Vigo, Spain

***Heriot-Watt University, Edinburgh, Edinburgh EH14 4AS, UK*

Associate Editor – Catherine Reid

ABSTRACT

Interbedded contourites, turbidites and pelagites are commonplace in many deep-water slope environments. However, the distinction between these different facies remains a source of controversy. This detailed study of calcareous contourites and associated deep-marine facies from an Eocene–Miocene sedimentary succession on Cyprus clearly documents the diagnostic value of microfacies in this debate. In particular, the variability of archetypical bi-gradational contourite sequences and their internal subdivision (bedding, layering and lamination) are explored. Contourites can be distinguished from turbidites, pelagites and hemipelagites by means of carbonate microfacies in combination with bed-scale characteristics. Particle composition provides valuable information on sediment provenance. Depositional texture, determined by the ratio between carbonate mud and bioclasts, is crucial for identifying bi-gradational sequences in both muddy and sandy contourites, and normally-graded sequences in turbidite beds. Equally important are the type and preservation of traction structures, as well as the temporality and impact of bioturbation. Shell fragmentation under conditions of increased hydrodynamic agitation (textural inversion) is recognized as a carbonate-specific feature of bioclastic sandy contourites.

Keywords Carbonate microfacies, continental slope, contourites, Cyprus, deep-marine deposits, pelagites, turbidites.

INTRODUCTION

The interaction of downslope and alongslope processes is the norm on many continental margins, resulting in the accumulation of interbedded turbidites, contourites and associated deep-water facies, in particular in carbonate environments (Eberli & Betzler, 2019; Mulder *et al.*, 2019). The rugged topography of many carbonate provinces causes heterogonous interaction between bottom currents and carbonate buildups, and large downslope gravity systems deliver sediment from the adjacent platform margin to the contour current via multiple sources. However, the nature of this interaction and, in particular, the distinction between

different facies types remains poorly understood, despite many decades of research (for example, compare Stow, 1979, with Rebesco *et al.*, 2014). The issue has become more critical recently due to the recognition of sandy contourites as potential hydrocarbon reservoirs (Viana, 2008; Shanmugam, 2012), and by the interpretation of several existing oil and gas fields as being reservoired in bottom-current reworked turbidites (e.g. Shanmugam *et al.*, 1993; Famakinwa *et al.*, 1997; Moraes *et al.*, 2007; Viana *et al.*, 2007; Palermo *et al.*, 2014; Decalf *et al.*, 2016; Huang *et al.*, 2017; Sansom, 2017; Ferguson *et al.*, 2018; Fuhrmann *et al.*, 2018; Fonnesu *et al.*, 2020). In fact, there is still much controversy over the criteria by which contourites, especially sandy contourites, can be recognized and distinguished from turbidites (see Hüneke & Stow, 2008; Martín-Chivelet *et al.*, 2008; Rebesco *et al.*, 2008; Shanmugam, 2008, 2017, 2018; Rebesco *et al.*, 2014; Castro *et al.*, 2020).

In principle, the distinction might be considered straightforward. Turbidites are event beds, deposited 'instantaneously' by generally downslope-directed gravity currents. They are characterized by normal grading, a standard sequence of structures, and top-down bioturbation. Primary sedimentary structures (parallel and cross-lamination) are mostly well-preserved. By contrast, contourites are the result of semi-continuous accumulation, involving both multiphase particle entrainment and deposition accompanied by persistent bioturbation. Contourite accumulation is incremental and may repeatedly change between bed-load-dominated and suspension-load-dominated deposition, including episodes of erosion and winnowing (McCave, 2008; Stow *et al.*, 2008). Bioturbation is penecontemporaneous with sedimentation and its intensity varies mainly due to changing hydrodynamic conditions and food supply, favouring or suppressing burrowing benthic communities (Wetzel *et al.*, 2008; Rodríguez-Tovar & Hernández-Molina, 2018). Bi-gradational sequences (inverse to normal grading) are common, and primary sedimentary structures may be partly or completely obliterated by bioturbation.

However, it is also known that parallel-lamination, cross-lamination and dune cross-bedding may be preserved in sandy contourites that have been deposited under conditions of short-term higher accumulation rates and lower bioturbation intensities (Martín-Chivelet *et al.*, 2008; Stow *et al.*, 2013; Capella *et al.*, 2017; Brackenridge *et al.*, 2018; Castro *et al.*, 2020). This paper addresses the detailed nature of, and distinction between, interbedded deep-water facies from a well-exposed and intensively studied carbonate slope succession in southern Cyprus. This study suggests that the microfacies and bed-scale diagnostic criteria identified have widespread application to slope deposits worldwide.

The calcareous succession of the Lefkara and Pakhna formations in Cyprus, accumulated during the Eocene to middle Miocene as a deep-water palaeoslope system (Fig. 1), comprising turbidite, contourite and pelagite–hemipelagite facies (Robertson, 1990; Stow *et al.*, 1995; Kahler & Stow, 1998). Because of its excellent and easily accessible exposure, as well as clear evidence for deposition from alongslope bottom currents, the area around Petra Tou Romiou has been proposed as a type example of ancient contourites exposed on land (Robertson, 1976, 1977; Kahler & Stow, 1998; Stow *et al.*, 2002). Many sedimentologists have since examined the deep-sea sediments in this region and agree that bottom-current deposits form at least a substantial part of this record (e.g. Hüneke & Stow, 2008; Rebesco *et al.*, 2014; Rodríguez-Tovar & Hernández-Molina, 2018; Papadimitriou *et al.*, 2018; Eberli & Betzler, 2019; Reolid & Betzler, 2019; Miguez-Salas & Rodríguez-Tovar, 2019a; Miguez-Salas *et al.*, 2019a; Rodríguez-Tovar *et al.*, 2019a; Miguez-Salas & Rodríguez-Tovar, 2019b; Rodríguez-Tovar *et al.*, 2019b). The identification of these deposits as contourites is based on careful consideration of the different scales and criteria (evidence at outcrop, regional evidence and palaeogeographic setting) and follows the three-stage approach to identification, as first proposed by Lovell & Stow (1981) and refined by Stow *et al.* (1998).

This Cypriot succession is one of the best-known and most well-established fossil contourite series in the world. This very detailed study documents for the first time the nature of close interbedding of turbidite and pelagite–hemipelagite facies with the dominant contourites in this succession. This approach uses their small-scale characteristics and, in particular, carbonate microfacies analysis for differentiating more precisely between contourites, turbidites and pelagites, which all typically contribute, to different degrees, to the formation of a contourite depositional system (CDS). Sediment provenance, depositional processes and post-depositional changes are interpreted based

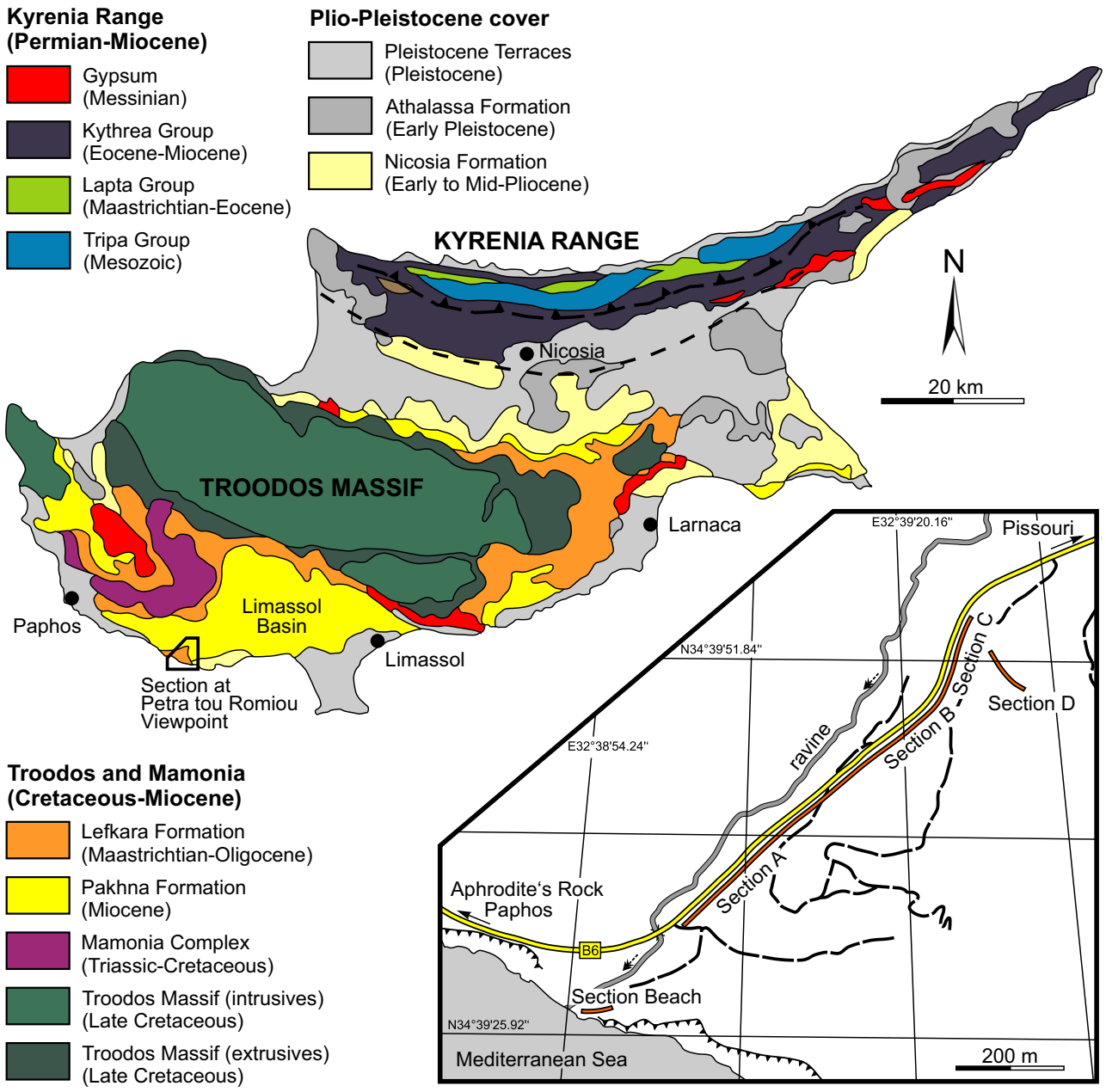

Fig. 1. (A) Summary geological map of Cyprus showing the Circum Troodos Massif sedimentary succession (modified from Constantinou, 1995; Palamakumbura & Robertson, 2018); and (B) location of the study area. Note the distribution of the Lefkara and Pakhna formations.

on particle composition, depositional textures and sedimentary structures. Hydrodynamic interpretation is based on depositional textures and grain-size variation, and considers carbonate-specific sediment properties (McCave & Hall, 2006; Eberli & Betzler, 2019). The well-exposed sedimentary record of the Lefkara and Pakhna formations offers a unique opportunity to identify and evaluate the most useful outcrop-scale and microfacies criteria for the identification of calcareous bottom-current deposits. These criteria will consequently act as a basis for distinguishing more precisely between bottom-current and gravity-flow deposits in sediment cores obtained by both marine geology cruises and drilling expeditions.

GEOLOGICAL AND PALAEOCEANOGRAPHIC SETTING

The deep-marine record of the Lefkara and Pakhna formations, which are essential units of the Circum Troodos sedimentary succession on Cyprus (Fig. 1), is widespread in the Limassol Basin (Papadimitriou *et al.*, 2018; Khalassa Basin according to Eaton & Robertson, 1993). The **Lefkara Formation** (Pantazis, 1967; Mantis, 1970) has been deposited during late Cretaceous to early Miocene above oceanic crust formed during the late Cretaceous (Sanfilippo *et al.*, 2003; Peybernes *et al.*, 2005). It rests unconformably on basaltic pillow lavas of the Troodos ophiolite (Cenomanian–Turonian) or on volcaniclastic sandstones and benthonitic clays of the Kannaviou Formation (Campanian) (Robertson & Hudson, 1974). Based on a detailed micropalaeontological study, Peybernes *et al.* (2005) demonstrated that the base of the Lefkara Formation is related to a stratigraphic hiatus and revealed a diachronous onset of the pelagic sediment accumulation.

The Lefkara Formation mainly consists of chalky limestones and marls with intercalations of bedded and nodular cherts (Moores & Vine, 1971; Robertson & Hudson, 1974; Robertson, 1990; Edwards *et al.*, 2010). Lower, Middle and Upper lithostratigraphic subunits are distinguished (Kahler & Stow, 1998): (i) lower marls (Palaeocene–Eocene); (ii) chalks and cherts (Eocene–Oligocene); and (iii) upper marls (Oligocene–Miocene). This carbonate-dominated succession formed partly by pelagic and hemipelagic sediment accumulation, in part by the significant influence of bottom-currents (Robertson, 1976, 1977; Kahler, 1994; Kahler & Stow, 1998; Stow *et al.*, 2002) and punctuated by distal turbidity flows. Based on these authors, deposition of this deep-marine record occurred on the continental slope, located in the southern periphery of Cyprus. Estimates of palaeowater depth based on sediment facies, microfossil assemblages and preservation suggest depths in the range of 2000 to 3000 m (Kahler, 1994). Robertson (1977) identified *in situ* benthic foraminifera and recognized a gradual shallowing of the region since the Late Eocene.

The subsequent **Pakhna Formation**, which overlies the Lefkara Formation, disconformably in most areas (Eaton & Robertson, 1993), has been deposited during the early to late Miocene. It continues with a deep to shallow-marine carbonate-dominated record, which shows transition to reef and other shallow-water carbonates of the Terra and Koronia members (Mantis, 1970; Follows, 1992; Constantinou, 1995). The deep-marine facies was formed by pelagic and hemipelagic sediment accumulation that experienced upward increased input of both shallow-water bioclastic sediments and ophiolite-derived siliciclastic components. Supply of bioclastic materials has been maintained by a broad range of gravity processes such as slides, slumps and density flows (Eaton & Robertson, 1993; Lord *et al.*, 2009). The latter included debris flows, hyperconcentrated and concentrated density flows, and turbidity flows, which produced various types of calcarenitic and calciruditic deposits. In addition, the deep-marine sedimentation was progressively controlled by bottom-currents that formed calcilutitic and calcarenitic bioclastic contourites (Hernández-Molina *et al.*, 2018), all of which were initially attributed to the Lefkara Formation (Kahler, 1994; Kahler & Stow, 1998; Stow *et al.*, 2002).

Plate-tectonic processes controlled the regional geological setting for sedimentation starting with collision of the Mamonia and Troodos terranes, both being overlain by the Lefkara Formation, and subsequent uplift of the Troodos ophiolite complex, and finally the migration of the subduction zone to the south of the island (Robertson & Woodcock, 1979). The Pakhna Formation was related to onset of the northward subduction of the African plate beneath Cyprus as well as continuing uplift and emersion of the Troodos ophiolite complex (Eaton & Robertson, 1993). The collision with the Kyrenia Range in the north occurred during the Pliocene to Pleistocene (Palamakumbura & Robertson, 2018; Papadimitriou *et al.*, 2018).

During early to middle Miocene, the Limassol Basin in southern Cyprus (Fig. 1) formed as a flexural basin under conditions of the compressive regime described above (Eaton & Robertson, 1993; Papadimitriou *et al.*, 2018). The geometry and bathymetry of the basin and thus the sedimentation were controlled by the thrust-bounded margin of the Troodos Complex in the north (Yerasa Fault System), a subparallel (WNW-trending) thrust fault system to the south (Akrotiri High) and an oblique ramp to the west (Xeropotamos transverse zone). The depositional environment changed from a deep slope at a depth probably more than 2000 m during the early Eocene to an intra-slope basin less than

500 m deep during the early Miocene, which was estimated on the basis of microfossil assemblages, trace fossil associations and sediment facies (Eaton & Robertson, 1993; Kahler, 1994; Stow *et al.*, 2002; Papadimitriou *et al.*, 2018). Shallow-water bioclastic sediments, including reef talus, were supplied by gravity flows from intrabasinal shoals along blind-front thrusts within and at the southern margin of the Limassol Basin (Eaton & Robertson, 1993).

The palaeoceanographic setting of the eastern Mediterranean area has been a further influential factor, particularly with regard to intensification of bottom-current flow west of the closing Indian gateway (Stow *et al.*, 2002). The closing Tethys Ocean (Proto-Mediterranean Sea) was connected to both the Atlantic and Indian Oceans during the Palaeocene–Oligocene and during much of the early Miocene (Rögl, 1999; Meulenkamp & Sissingh, 2003; Harzhauser *et al.*, 2007; Reuter *et al.*, 2009). Both the gateway to the Indian Ocean and the Atlantic Gateway accommodated a net westward flow (Jovane *et al.*, 2009; Butzin *et al.*, 2011; Krapp & Jungclaus, 2011; Herold *et al.*, 2012). This warm surface current is often considered the result of a west-directed circum-equatorial current, the so-called 'Tethys Circumglobal Current', which has been inferred from biogeographic evidence and modelling studies (Hallam, 1969; Stanley, 1995; Bush, 1997; Omta & Dijkstra, 2003; Heydt & Dijkstra, 2006).

The oceanographic models infer a large anticlockwise circulation cell in the region of the Tethys Ocean that is now the eastern Mediterranean. This circulation extended down to the bottom of the oceanic basin and drove an east-directed bottom-current system, which has been modulated by this west-directed net flow (Vara & Meijer, 2016). A powerful net flow weakened this cell when the Indian Gateway was deep (Eocene–Oligocene), whereas the cell strengthened when the gateway was shallow (early Miocene).

Oligocene to early Miocene shoaling of the gateway to the Indian Ocean, which is caused by the collision of the Arabian plate with the Eurasian plate, triggered intensification of both the westward surface flow within the Indian gateway and the eastward bottom flow within the eastern Mediterranean deep sea (Vara & Meijer, 2016). The final closure of the Indian Gateway occurred around the middle Miocene after several short-lived cessations during the early Miocene (Rögl, 1999; Harzhauser *et al.*, 2007).

INVESTIGATED OUTCROP, MATERIAL AND METHODS

In this investigation, the sedimentary record has been studied at the locality Petra Tou Romiou (Fig. 1), which exposes the Middle and Upper Lefkara Formation and the Pakhna Formation (Fig. 2) within the south-western Limassol subbasin (Pissouri Basin, Fig. 1A). The carbonate-dominated succession is accessible along a road cut of the B6 between Pissouri and Aphrodite's Rock (Fig. 1B). A 200 m thick sedimentary record has been studied and logged from the sea cliff at the lower end of the valley (34°39'27.52″N, 32°38'56.31"E), along the road (from 34°39′32.65″N, 32°39′1.78″E to 34°40′0.16″N, 32°39′34.10″E) and up to the hill south-east of the road (34°39′50.33″N, 32°39′29.69″E). The focus of this paper is on carbonate microfacies of the Eocene to middle Miocene part of the succession.

The studied material includes 80 thin sections from the Petra Tou Romiou section, most of them prepared at a size of 7 × 10 cm in order to document sedimentary structures and microfacies variation at the bed scale. In addition, four sections exposing parts of the Lefkara and Pakhna formations in other areas of the Circum Troodos Massif sedimentary succession (Agios Konstantinos, Zenon, Korfi and Kalavasos) were studied for comparative purposes. The Petra Tou Romiou section has been logged bed by bed and numbered from bottom to top during several field campaigns conducted between 2014 and 2017. Samples for thin sections have been obtained from all lithologies and from all parts of the measured sections. Individual key beds have been documented with up to eight thin sections to investigate subtle facies variations across the beds and along their lateral continuation, in particular transitions across bed boundaries into the underlying and overlying lithologies.

Since this investigation focuses on contourites and their differentiation from turbidites and pelagites, microfacies types are primarily defined by grain size and depositional texture, supplemented by compositional criteria and sedimentary structures. Grain-size distribution and sorting are crucial for a process-based environmental interpretation of allochthonous carbonates, which do not result from *in situ* production of skeletal grains, but from grain-size-related selective particle deposition and winnowing of mud (Flügel, 2010). Consequently, the terms

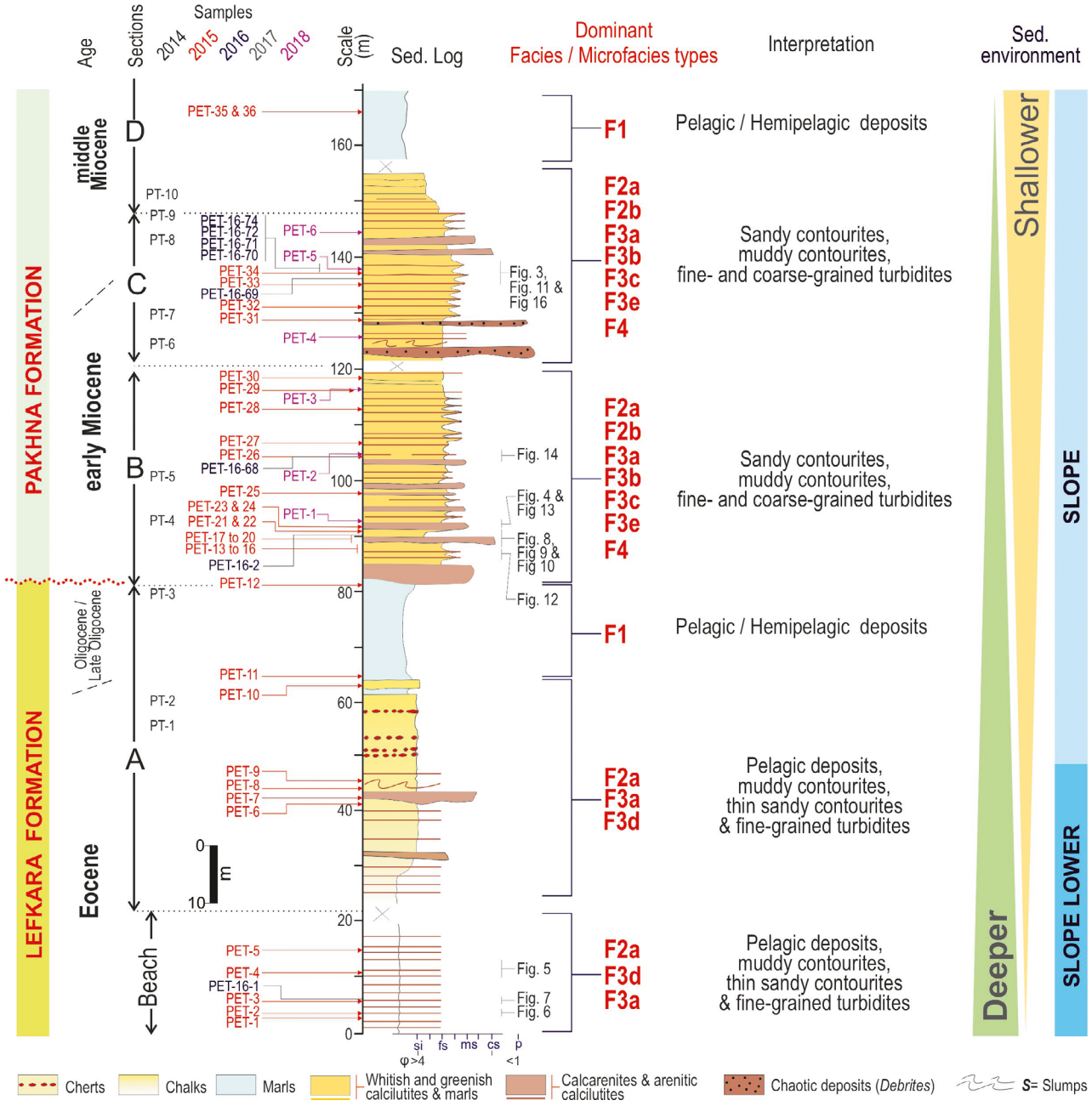

Fig. 2. Simplified sedimentary log of the late Eocene to middle Miocene Lefkara and Pakhna formations recorded at Petra Tou Romiou. Ages, dominant facies and microfacies are reported for each section (dominant and subordinate facies are indicated in bold and normal red, respectively). A brief interpretation and the decoded sedimentary environments are also included. The relative position of each figure is shown for better understanding of the vertical facies changes.

calcilutite (micrite), calcisiltite, calcarenite and calcirudite are used (Grabau, 1904; Kay, 1951; Folk, 1959) to refer to the complete range of contourite facies (Stow & Faugères, 2008; Rebesco *et al.*, 2014) in combination with textural classification (Dunham, 1962; Embry & Klovan, 1972). The abundance of grains and the grain types are of similar prime importance in defining microfacies types and allow the discrimination of source areas for allochthonous carbonates. Additional environmentally sensitive criteria, which were used to identify specific transport and

depositional processes, are primary sedimentary structures such as particle grading, cross-lamination and wavy lamination.

Grain size and sorting were generally estimated using visual comparison charts (Longiaru, 1987). Quantitative data are derived from key samples of all microfacies types only; the exemplary grain-size measurements and histogram plots are based on areal percentages in thin sections using gridded microphotographs (238 squares per 200 × 200 μm and 238 squares per 50 × 50 μm). Mean grain size was calculated based on the equation of Folk & Ward (1957). The identification of foraminifera is mainly based on work of Iaccarino & Premoli Silva (1979), Chaisson & Leckie (1993), Pearson & Chaisson (1997), Hicks (2014) and Hesemann (2018), and derived enormous benefit from the mikrotax.org and the foraminifera.eu internet projects (see Hesemann, 2015). The relative percentage frequency of different components has been determined by means of the visual-comparison charts of Baccelle & Bosellini (1965) and Matthew *et al.* (1991).

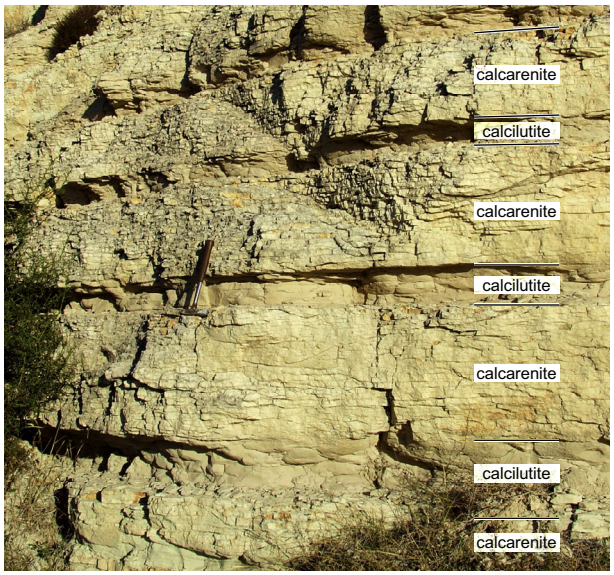

Fig. 3. Example of regular, distinct decimetre-scale cyclicity produced by interstratified whitish calcilutite (F2a, globigerinid wackestone) and wavy-layered calcarenite beds (F3b, globigerinid packstone–grainstone). Middle Miocene from the Pakhna Formation as part of Petra Tou Romiou section (Sample Pet 34). Note hammer for scale (32 cm in length).

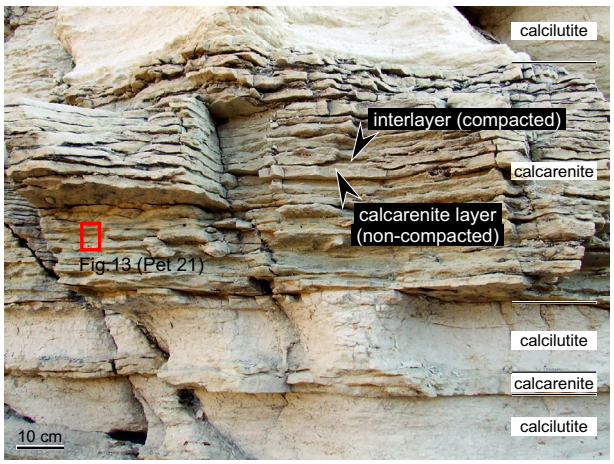

Fig. 4. Example of irregular, clear decimetre-scale cyclicity formed by alternating beds of whitish calcilutites (F2a, globigerinid wackestone) and wavy-layered greenish calcarenites (F3c, globigerinid packstone–grainstone). Early Miocene from the Pakhna Formation as part of Petra Tou Romiou section. Red rectangle indicates sampling point for thin section Pet 21. See Fig. 13 for details of the depositional texture and microfacies.

RESULTS

Lithologies and stratigraphic overview

Chalky calcilutites and marls with individual thin calcarenite beds and chert layers dominate the lower part of the studied record (Fig. 1, Section Beach and Section A). The upper part is made up of chalky calcilutites and thick calcarenite beds of almost equal quantities (Fig. 1, Sections B and C). A marl-rich interval, with an indistinct unconformity at its top, separates the two parts of the section (Fig. 2). A notable thick calcirudite bed occurs about 8 m above this unconformity.

There is a clear decimetre to metre-scale cyclicity caused by interstratified calcilutite and calcarenite beds within the early and middle Miocene part of the record, i.e. the upper part of the studied section (Figs 3 and 4). Although subtle, a centimetre to decimetre-scale grain-size related cyclicity is also developed in the Eocene, i.e. lowermost part of the studied succession (Fig. 5).

Facies and microfacies

Based on bed-scale sedimentary characteristics and carbonate microfacies, nine facies have been typified which are expressed in certain lithologies (Table 1). Marls (F1) mainly constitute the middle and uppermost parts of the studied

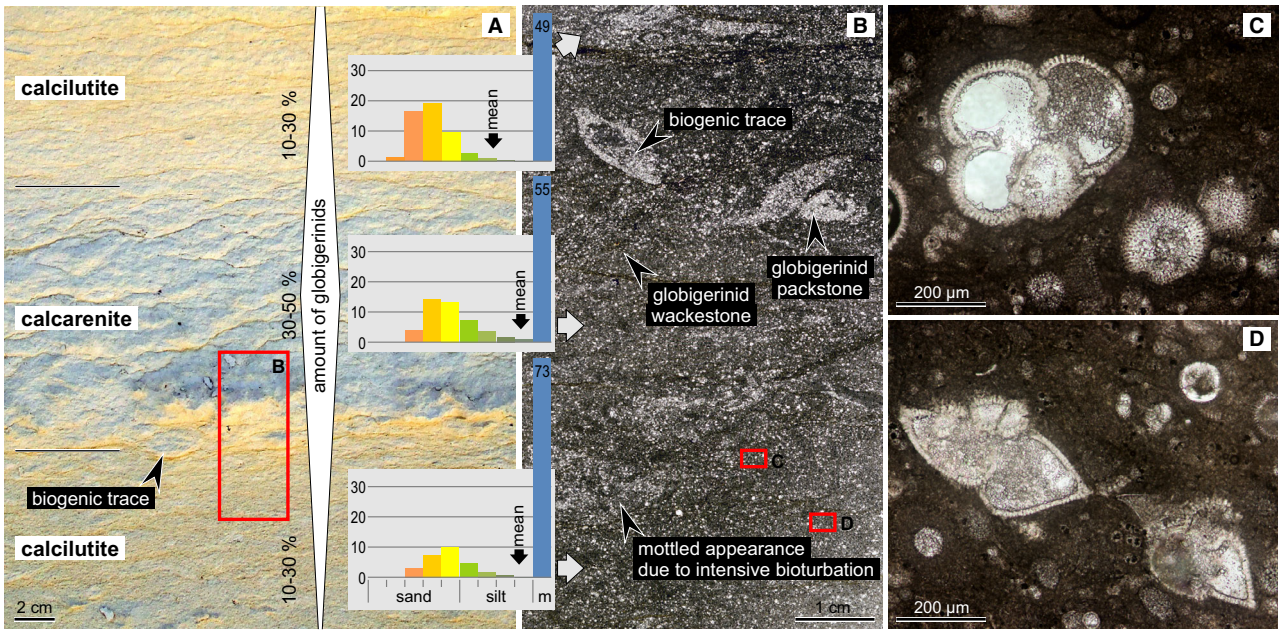

Fig. 5. Whitish calcilutites (F2a, globigerinid wackestone) interstratified with a thin whitish calcarenite bed (F3a, globigerinid wackestone–packstone). Interpretation: Mud-dominated bi-gradational contourite sequences C1–(C2)–(C4)–C5. Eocene from the Lefkara Formation as part the of Petra Tou Romiou section (Sample Pet 4u). (A) The mud-rich calcilutites are more prone to weathering and appear more homogeneous. Rhombus highlights gradual mean grain-size variation. (B) Thin-section scan showing gradual transition from calcilutite to calcarenite. Histograms document decrease of mud in favour of globigerinid shells (mean grain-size shift from fine silt to coarse silt). The sediment is mottled due to intensive bioturbation. Note the district biogenic traces (filled with globigerinid packstone). (C) Planktonic foraminifera are mainly globigerinids characterized by globular chambers. (D) Planktonic foraminifera of the keeled globorotaliids occur rarely.

record (Fig. 2). Although remnants of planktonic foraminifera are preserved within these marls, its microscopic fabric is strongly affected by pressure dissolution. Primary sedimentary structures (traction structures and grading) and secondary structures (biogenic traces) are partially obscured by chemical compaction. Consequently, they are not considered in detail from the viewpoint of carbonate microfacies analysis.

Whitish calcilutite: globigerinid wackestone (F2a)

Whitish calcilutite is the main lithology of the studied record. Macroscopically, the facies is characterized by an apparently homogeneous fabric (Figs 4 and 5). However, on closer inspection, polished slabs and thin sections display a diffuse mottled appearance resulting from intensive bioturbation. The sediment displays a crude bedding marked by decimetre-thick bioturbated beds alternating with more structureless, less-bioturbated beds. At numerous stratigraphic levels, distinct traces can be recognized, which are typically filled by calcareous sediment with differing grain size or slightly divergent colour. A recent ichnological analysis reveals a trace fossil assemblage consisting of *Chondrites* isp. (*C. intricatus* and *C. targionii*), *Planolites* isp., *Taenidium* isp. and *Zoophycos* isp. (Miguez-Salas & Rodríguez-Tovar, 2019a; Rodríguez-Tovar *et al.*, 2019a).

Microfacies. These calcilutites are wackestone beds comprising almost exclusively planktonic foraminifera of the family Globigerinidae (Fig. 5). The distinctly perforate trochospiral tests composed of hyaline calcite, with globular chambers are ubiquitous. Other skeletal grains such as smaller benthic foraminifera, thin-shelled brachiopods and molluscs are extremely rare. The carbonate mud is nannofossil micrite, made up of coccolithophorids (coccoliths) and other calcareous nannoplankton.

The planktonic foraminifera are of different sizes and unevenly distributed, which is interpreted here as the result of intense biogenic

Table 1. Main sedimentary characteristics and lithologies of the facies typified within the Eocene to middle Miocene record of the Lefkara and Pakhna formations at Petra Tou Romiou on Cyprus and interpretation of relevant depositional processes.

FACIES TYPES			SEDIMENTARY STRUCTURES		MICROFACIES		ICHNOLOGY	DEPOSITIONAL PROCESS	
F1	MARLS		Lamination				Intensive bioturbation	PELAGIC / HEMIPELAGIC	
F2a	CALCILUTITES (Chalks)	Whitish	Primary sedimentary structures not recognized. Biogenic structures (e.g. burrows)		*Globigerinid wackestone* (planktonic foraminifera are ubiquitous). Other rare biogens: smaller benthic foraminifera, thin-shelled brachiopods and molluscs. The carbonate mud is nannofossil micrite (calcareous nannoplankton; coccoliths)		Intensive bioturbation, sometimes discrete burrows difficult to be differentiated from the host sediment; diffuse mottled appearance	Pelagic carbonate mud/ calcareous *muddy contourites* (reworking of pelagic sediments)	PELAGIC / CONTOURITE
F2b		Greenish	*See above*		*See above* Enriched in illite, with contents of 2–3%		Intense bioturbation but easier differentiation of discrete burrows. Diffuse mottled appearance	Calcareous *muddy contourites* (reworking of pelagic sediments and clays from altered ophiolites)	
F3a	CALCARENITES	Thin whitish beds with gradational boundaries	Central part of a bi-gradational sequence (C3); faint wavy lamination		*Globigerinid wackestone–packstone* (packed biomicrites and poorly washed biosparites). The globigerinid tests are well-preserved		Heavily bioturbated. Diffuse bioturbational mottling. Discrete biogenic structures occur	Bioclastic *sandy bottom-current deposits* (reworking of pelagic sediments)	CONTOURITES
F3b		Whitish beds with internal wavy layering	Bed boundaries are indistinct and show gradual transition to whitish and greenish calcilutites. Distinctly layered	*(a) Non-compacted layers* = homogeneous or bioturbationally-mottled texture; faint parallel and cross lamination is locally preserved. Even more rarely, bed-form related relic morphologies occur.	*Globigerinid packstone-grainstone with varying (low) amounts of shallow-water bioclasts*. Biogenic activity clearly influenced the preserved fabric	*(a) Non-compacted layers* = Globigerinids are the main constituents, with well-preserved tests. Fragmented shallow-water bioclasts of similar grain size (with layer-specific amount) may occur	–	Bioclastic *sandy bottom-current deposits* (reworking and redistribution of pelagic sediments and turbidites); formed: (a) during short-term flow acceleration causing intensification of rippled-bed traction; (b) during short-term flow deceleration causing dumping of suspended sediment	
				(b) Compacted interlayers = pressure-dissolution seams		*(b) Compacted interlayers* = fragmented and flattened tests prevail within the compacted laminae. Higher content of fine-grained materials such as micrite and clay minerals	Diffuse bioturbational mottling and scarce discrete biogenic traces occur		
F3c		Greenish beds with internal wavy layering	*See above*		*See above* Enriched in illite, with contents of 2–3%		*See above*	Bioclastic *sandy bottom-current deposits* (reworking of pelagic sediments, turbidites, and altered ophiolites)	
F3d		Thin, sharp-based beds	Sharp-based/gradual top boundary into calcilutites (F2a). Fining-upward sequences (*normal grading*). Well-preserved primary traction structures (parallel and low-angle cross lamination)		*Globigerinid grainstone to wackestone*. Planktonic foraminifera occur almost exclusively (Globigerinidae). Particle-supported fabrics in lower part		Upper part of the bed intensively bioturbated by discrete traces. Mottled appearance not observed	Fine-grained turbidites sourced from slope settings. Reworked and dislocated pelagic sediments only	TURBIDITES
F3e		Sharp-based beds with normal grading	Distinct *normal grading; s*harp-based/ gradual top [or sharp and irregularly truncated upper surface overlain by calcarenites (F3b,c)]		*Larger-benthic-foraminifera globigerinid packstone* (more rarely grainstone). The bioclastic fraction shows a balanced ratio of both (well-preserved) planktonic foraminifera and (fragmented) shallow-water materials of similar grain size. The latter include larger benthic foraminifera. Intraclasts at the base of the normally-graded beds		Discrete biogenic structures are recognized	*Turbidites* sourced from shallow-marine carbonate and upper slope settings. [top reworked by bottom currents]	
F4	CALCIRUDITES	Sharp-based structure-less beds	Planar and sharp base/top gradual to calcilutites (F2a,b), forming fining-upward sequences [or truncated by calcarenites (F3b,c)]; locally wavy lamination and cross-bedding		*Larger-benthic-foraminifera corallinacean rudstone*. The beds consist of bioclastic materials from euphotic shallow-water sources (larger benthic foraminifera, corallinacean red algae). <10% of the planktonic foraminifera (Globigerinidae). Intraclasts occur mainly within the lowermost part of the beds. Larger elongated bioclasts are parallel to bedding		Discrete traces difficult to observe	Coarse-grained *turbidites* sourced from shallow-marine carbonate environments [top reworked by bottom currents]	

Grey shade highlights contourite facies. Blue colour highlights main lithologies. Red colour highlights main types of sedimentary processes.

activity (Fig. 5). Circular patches, caused by burrows, may comprise mudstone or globigerinid packstone texture and result from the refilling of biogenic traces.

The vast majority of the spherical tests are well-preserved. Fragmented tests are typically associated with traces and are mainly the result of biogenic activity (Fig. 6D). The tests are filled with micrite (carbonate mud) or sparite (calcite cement) or they are unfilled (intra-particle porosity).

Greenish calcilutite: globigerinid wackestone enriched in illite (F2b)

Greenish calcilutite beds are more common in the upper part of the studied record. Their microfacies is almost identical to the whitish calcilutite (F2a). In contrast to the latter, however, they are enriched in illite and quartz, with contents of 2 to 3% as indicated by X-ray diffraction (XRD) analysis (Hernández-Molina *et al.*, 2018). Pressure dissolution seems to be more intense within the greenish calcilutites, most probably caused by the higher clay content.

Thin calcarenite beds with gradational boundaries: globigerinid wackestone–packstone (F3a)

Thin whitish beds of calcarenite, which have a thickness typically less than 5 cm, mainly occur in the lowermost part of the studied record (Fig. 2). Bed boundaries are indistinct and show gradual transition from and to whitish or greenish calcilutites, which typically occur below and above the calcarenite (Figs 5 and 6), signifying a gradual change in the depositional regime. Thicker representatives of these calcarenite beds (5 to 8 cm) may display a faint wavy lamination (Fig. 6A). Well-defined primary depositional structures are generally absent, in part because they have been thoroughly destroyed by bioturbation (Fig. 6B) or were modified by mechanical and chemical compaction.

At some stratigraphic levels, the calcarenite beds are characterized by lateral changes in thickness over a distance of several metres. They may even pinch out laterally, become replaced by a pressure dissolution seam, with calcarenite fillings of biogenic traces within the calcilutite interval present below. These are locally the only representative (relic) of this facies.

Microfacies. Thin calcarenite beds of this type typically consist of heavily bioturbated globigerinid wackestone–packstone (packed biomicrites and poorly washed biosparites) (Figs 5 and 6). Both diffuse bioturbational mottling and distinctly-bounded biogenic traces occur. The fragile globigerinid tests are mainly well-preserved. Local clusters of fragmented test are most likely related to biogenic traces (Fig. 6B) and indicate fragmentation caused by biogenic activity (Fig. 6C). Originating from the thin calcarenite beds, infill of globigerinid wackestone–packstone commonly plug biogenic traces that penetrate into the underlying calcilutites over a distance of a few decimetres (see Miguez-Salas & Rodríguez-Tovar, 2019a; Miguez-Salas *et al.*, 2019b).

Thin, sharp-based calcarenite beds with parallel and low-angle cross-lamination: globigerinid packstone–grainstone (F3d)

This facies mainly occurs within the lowermost part of the studied record (Fig. 2). The thickness of these sharp-based calcarenite beds is usually between 3 cm and 10 cm. The base is typically clear-cut and planar, whereas the top is indistinct and shows a gradual and irregular transition into calcilutite, which is most likely caused or masked by post-depositional burrowing (Fig. 7).

The lamination is mainly a well-defined planar parallel lamination, which may occasionally pass into a low-angle cross-lamination (Fig. 7B). This lamination is well-preserved within the lower part of the calcarenite beds only. The upper part of the thin calcarenite bed is intensively bioturbated. Laterally, the bioturbated upper part can become thicker at the expense of the laminated lower part.

Microfacies. Such calcarenite beds consist of globigerinid packstone and grainstone (Fig. 7). Planktonic foraminifera occur almost exclusively (Globigerinidae). The tests are mainly well-preserved. Particle-supported fabrics are the rule. In thin section, the lamination is defined by a stepwise variation in shell size of the accumulated globigerinids; whereas individual laminae are mainly well-sorted. Within the upper bioturbated part of the beds, areas with mud-supported and particle-supported textures are present.

Sharp-based structureless calcirudite beds: larger-benthic-foraminifera corallinacean rudstone (F4)

The structureless calcirudite beds are up to 50 cm thick (Fig. 8). Much thinner beds,

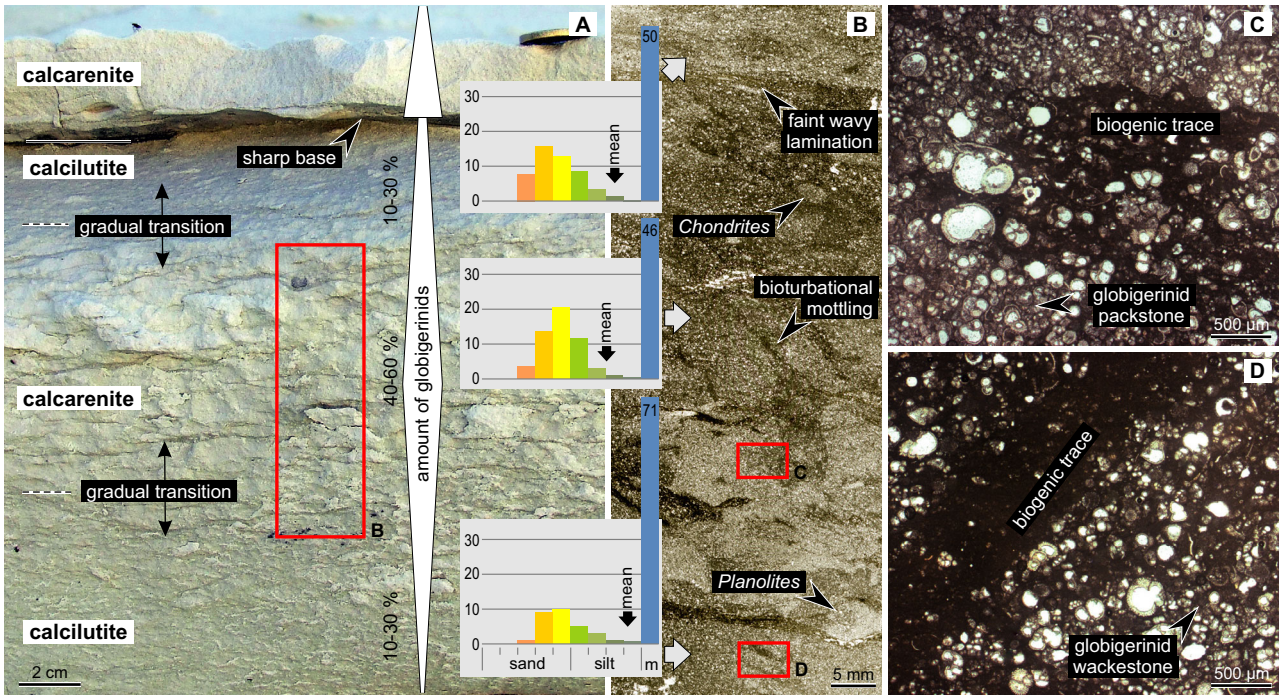

Fig. 6. Whitish calcilutites (F2a, globigerinid wackestone) interstratified with two different types of thin whitish calcarenite beds. Interpretation: Mud-dominated bi-gradational contourite sequences C1–(C2)–C3–(C4)–C5; overlain by fine-grained turbidite (see Fig. 7). Eocene from the Lefkara Formation as part the of Petra Tou Romiou section (Sample Pet 2u). (A) Note the two different types of calcarenite beds: The calcarenite in the central part of the photograph shows gradational boundaries (F3a, globigerinid packstone), while the laminated calcarenite in the upper part is sharp-based (F3d, globigerinid grainstone to wackestone; see Fig. 7 for details). Rhombus and triangle highlight mean grain-size variation. Coin for scale (24 mm in diameter). (B) Thin-section scan showing the intensive bioturbational mottling of the calcarenite with gradational boundaries. Note gradual transition from calcilutite to calcarenite and back to calcilutite. Histograms document decrease of mud in favour of globigerinid shells (mean grain-size shift from fine silt to coarse silt) followed by an increase of mud at the expense of globigerinid shells (mean grain-size shift from coarse silt to medium silt). (C) Calcarenite (globigerinid packstone) with biogenic trace (filled with globigerinid wackestone) (F3a). (D) Calcilutite (globigerinid wackestone) with biogenic trace (filled with globigerinid mudstone) (F2a).

however, also occur. The base is always planar and sharp, whereas the top may be sharp and distinct or gradual and irregular in lateral trend. Sharp upper boundaries occur where calcarenite beds with wavy layering (F3b and F3c) directly cover the structureless calcirudite beds. Gradual upper boundaries typify transitions to whitish or greenish calcilutites (F2a and F2b). Particle size is rather uniform, comprising pebble-sized and sand-sized calcareous bioclasts of different specific weights (porous and more massive skeletal elements). Normal size grading (or compositional grading) is mostly absent or restricted to the lowermost and uppermost part of the calcirudite beds. Crude wavy lamination and cross-bedding locally occur in lower part (Fig. 8).

Microfacies. The rudstones are dominated by robust bioclastic materials from euphotic shallow-water sources (Figs 9 and 10). Larger foraminifera and corallinacean calcareous red algae are ubiquitous. Further common skeletal remains of benthic organisms are bryozoans, thick-shelled brachiopods, crinoids, serpulids and (more rarely) colonial corals. The larger benthic foraminifera include *Amphistegina*, *Heterostegina*, *Operculina* and *Miogypsina*. In addition, there are tests of the planktonic foraminifera (Globigerinidae), which constitute less than 10% of all bioclasts. Calcareous intraclasts (globigerinid wackestone and globigerinid packstone) occur mainly within the lowermost part of the beds. Larger elongated bioclasts (larger foraminifera, brachiopods and corallinacean red

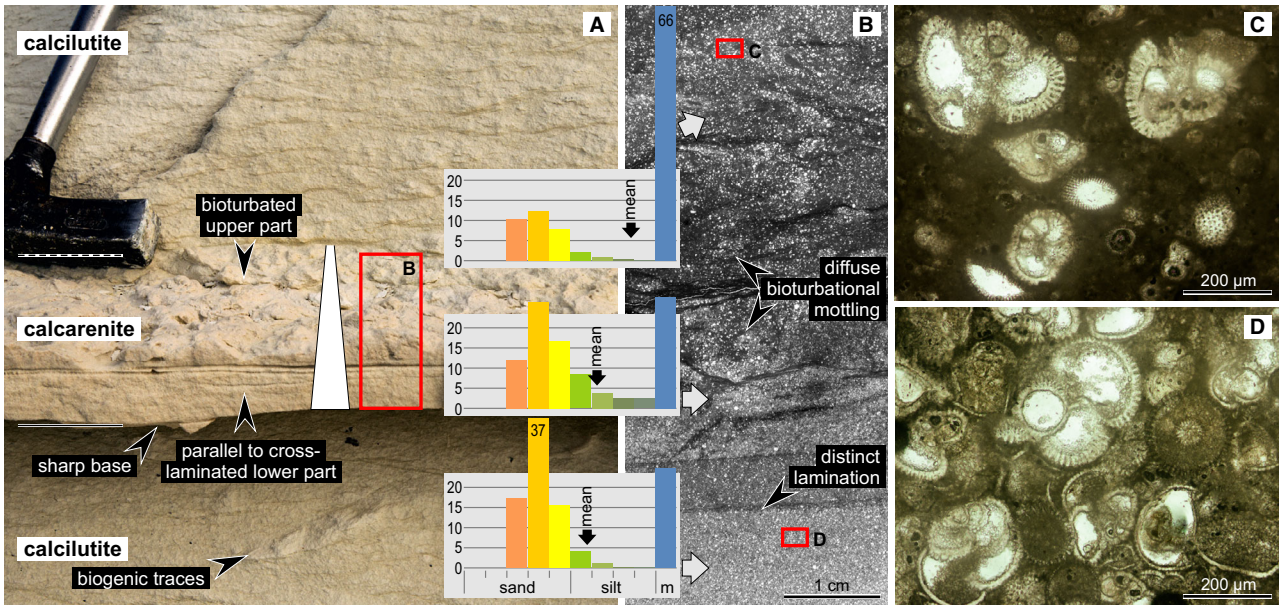

Fig. 7. Sharp-based calcarenite bed (F3d, globigerinid packstone to wackestone) within a succession of calcilutites (F2a, globigerinid wackestone). Interpretation: Fine-grained turbidite embedded between pelagic carbonates. Eocene from the Lefkara Formation as part the of Petra Tou Romiou section (Sample Pet 2016-1). (A) Note that the thin calcarenite bed preserves planar parallel lamination within its lower part (globigerinid packstone), while the upper part is heavily bioturbated (globigerinid wackestone). Triangle highlights mean grain-size variation of the calcarenite (normal grading). See hammer for scale (the hammer shaft is 1.8 cm in diameter). (B) Thin-section scan displaying the transition from laminated lower part to bioturbational-mottled upper part of the calcarenite (F3d). Histograms document an increase of mud at the expense of globigerinid shells (mean grain-size shift from very coarse silt to fine silt). (C) Calcarenite (F3d, globigerinid wackestone). (D) Calcarenite (F3d, globigerinid packstone).

algae) are commonly embedded with their long axes roughly parallel to bedding. Isolated sand-sized quartz grains occur scattered among the calcareous bioclasts.

Sharp-based calcarenite beds with normal grading: larger-benthic-foraminifera globigerinid packstone (F3e)

The sharp-based calcarenite beds showing distinct normal grading are commonly embedded within wavy-layered calcarenites (F3b and F3c). Bed thickness is typically less than 20 cm (for example, Fig. 11). Laterally, its planar and gradual upper boundary can be replaced by a sharp, irregular and erosive surface. Lamination is generally not discernible.

Microfacies. This facies consists of packstone and more rarely grainstone. Beds show a balanced ratio of both planktonic foraminifera and shallow-water materials of similar grain size. The latter include larger benthic foraminifera (*Amphistegina*, *Miogypsina*, *Heterostegina* and *Operculina*), benthic foraminifer (*Elphidium*), corallinacean red algae, crinoids, brachiopods and serpulids. Whereas the globigerinid tests are mostly well-preserved, the calcareous bioclastic debris supplied from euphotic shallow-water environments is largely fragmented (Fig. 11). Calcareous intraclasts (globigerinid wackestone and mudstone) occur at the base of the normally-graded beds.

Whitish calcarenite beds with internal wavy layering: globigerinid packstone–grainstone with varying (low) amounts of shallow-water bioclasts (F3b)

Calcarenite beds with well-developed wavy layering mainly occur within the middle and upper parts of the studied record (Fig 2). Bed thickness varies between 5 cm and 60 cm. Bed boundaries are indistinct and show gradual transition from and to whitish or greenish calcilutites (F2a and F2b), which typically occur below and above these calcarenite beds (Figs 3 and 4). Locally, at some stratigraphic levels, calcarenites with wavy

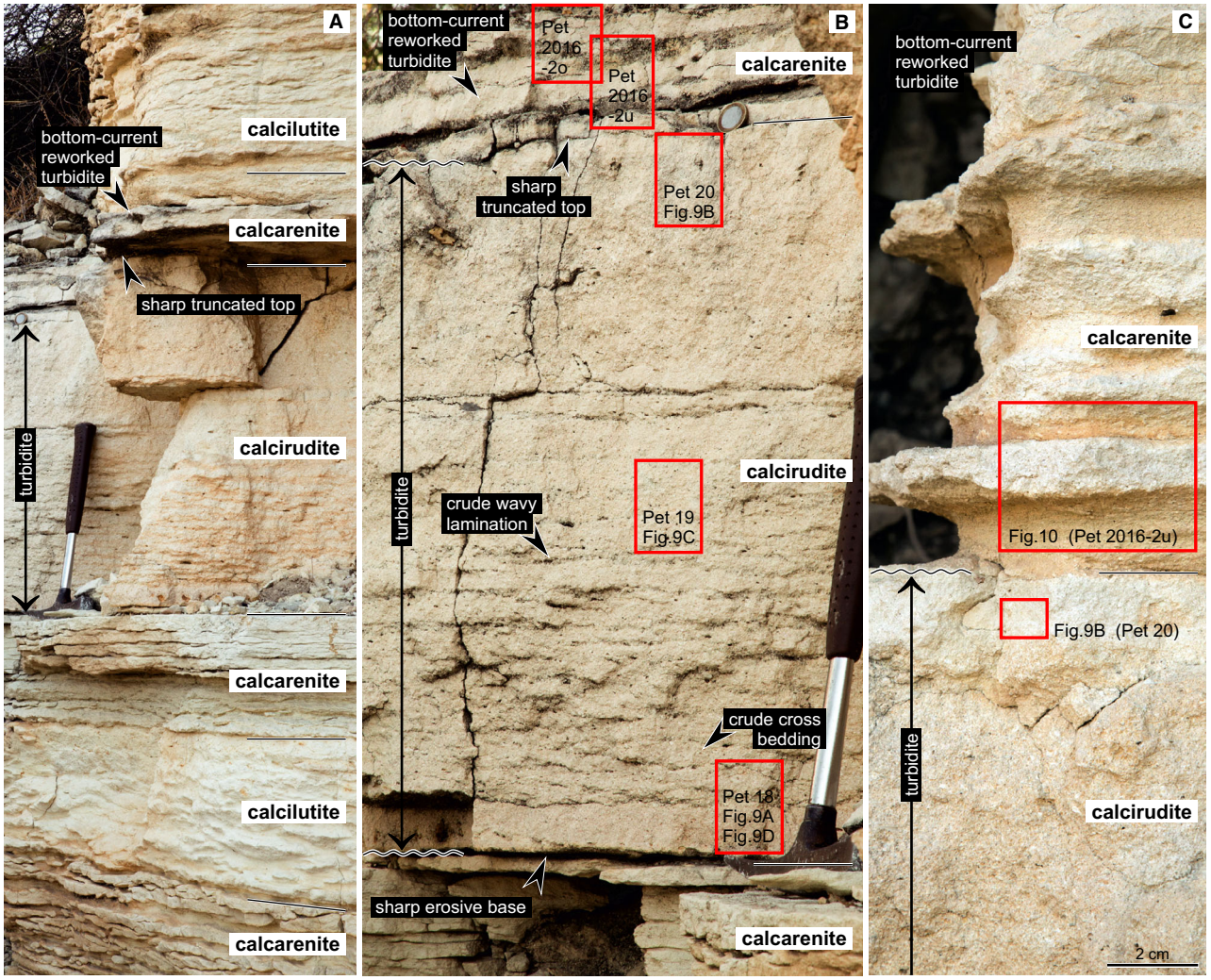

Fig. 8. Early Miocene from the Pakhna Formation as part of Petra Tou Romiou section. (A) Whitish calcilutites (F2a, globigerinid wackestone) interstratified with a sharp-based calcirudite bed (F4, larger-benthic-foraminifera corallinacean rudstone) and calcarenite beds with wavy layering (F3b and F3c, globigerinid packstone–grainstone with varying amounts of shallow-water bioclasts). See Figs 9 and 10 for depositional texture and microfacies. Red boxes show thin-section sampling points. Hammer for scale (32 cm long). Interpretation: Coarse-grained turbidite with reworked top interstratified between sand-dominated contourite sequences. (B) Detail of the sharp-based calcirudite bed, which mainly consists of benthic particles from euphotic carbonate environments (F4). Mainly based on the predominant shallow-water origin of its bioclastic components, it is interpreted as a turbidite. (C) Detail of the bottom-current reworked top of the turbidite bed. Note the massive and structureless appearance of the turbidite (F4) and the wavy layering of the bottom-current reworked part (transition to F3b).

layering cover and truncate structureless calcirudite beds (F4) along a sharp, distinct boundary (Fig. 11).

The internal sedimentary layering is the most striking feature (Figs 4 and 12), since it is very regular and eye-catching. The thickness of individual layers varies between 3 mm and 30 mm. It is mainly a continuous wavy layering that can be traced laterally without substantial variation. At some stratigraphic levels, it is replaced by a parallel planar layering or it shows a transition to non-parallel lenticular layering (Fig. 12). Rarely, poorly preserved cross-lamination is identified within individual layers.

Microfacies. At the microscopic scale, the wavy layering is defined by (indurated) non-compacted layers about 10 mm thick (varying between 3 mm and 30 mm) that are interstratified with thin (fissile) compacted interlayers (1 to 10 mm)

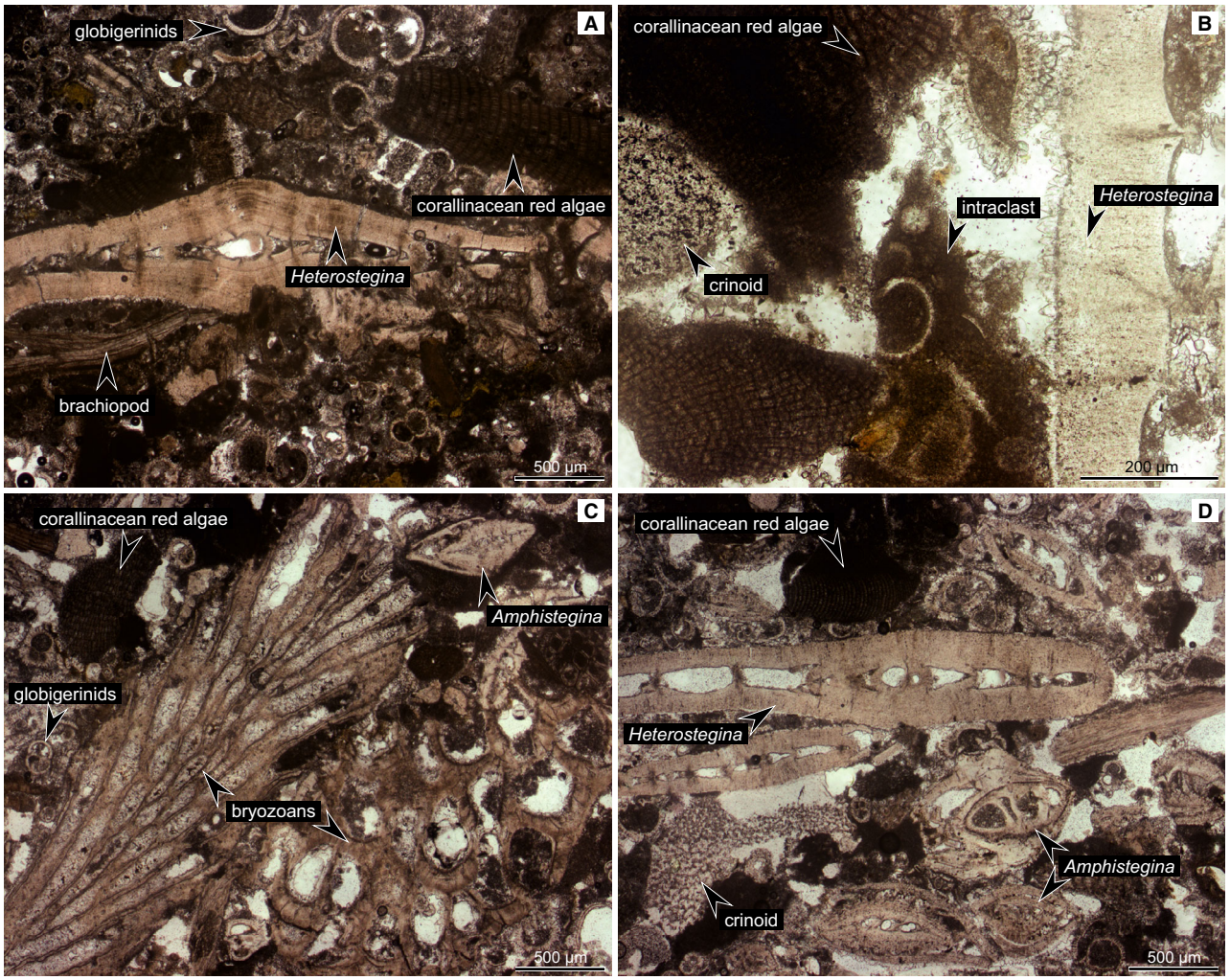

Fig. 9. Microfacies of the sharp-based calcirudite bed (F4, larger-benthic-foraminifera corallinacean rudstone) in the early Miocene (Pakhna Formation) as part of Petra Tou Romiou section (Samples Pet 18, 19 and 20). See Fig. 8B for general lithology and sampling points. Interpretation: shallow-water bioclasts (euphotic carbonate environments) of a coarse-grained turbidite. (A) Bioclastic rudstone rich in nummulitid larger foraminifera (*Heterostegina*) and corallinacean red algae (dark bioclasts with fine net-like structure). Note the subordinate amount of planktonic foraminifera (globigerinids). Thin section Pet 18. (B) Bioclastic rudstone including nummulitid larger foraminifera (*Heterostegina*), corallinacean red algae, crinoids and intraclasts (globigerinid wackestone). Thin section Pet 20. (C) Bioclastic rudstone comprising bryozoans, corallinacean red algae (dark bioclasts), larger benthic foraminifera (*Amphistegina*) and globigerinids. Thin section Pet 19. (D) Bioclastic rudstone consisting predominantly of larger benthic foraminifera (*Heterostegina* and *Amphistegina*), corallinacean red algae and crinoids. Thin section Pet 18.

(Figs 13 and 14). The former mainly consist of sand-sized intact globigerinids. The latter is largely made of fine sand to coarse silt-sized bioclastic fragments (essentially globigerinids) and reveal a slightly higher content of siliciclastic particles (shale lithoclasts and isolated quartz grains), which are interpreted as a primary depositional feature that has been enhanced by subsequent compaction and dissolution (Fig. 14). The non-compacted layers are typically characterized by a homogeneous or a bioturbational mottled texture without compactional features (for example, pressure dissolution seams). Locally, faint lamination or well-preserved parallel and cross-lamination may exist within the non-compacted layers. Even more rarely, bed-form (ripples and small dunes) related relic morphologies have been identified (Fig. 15).

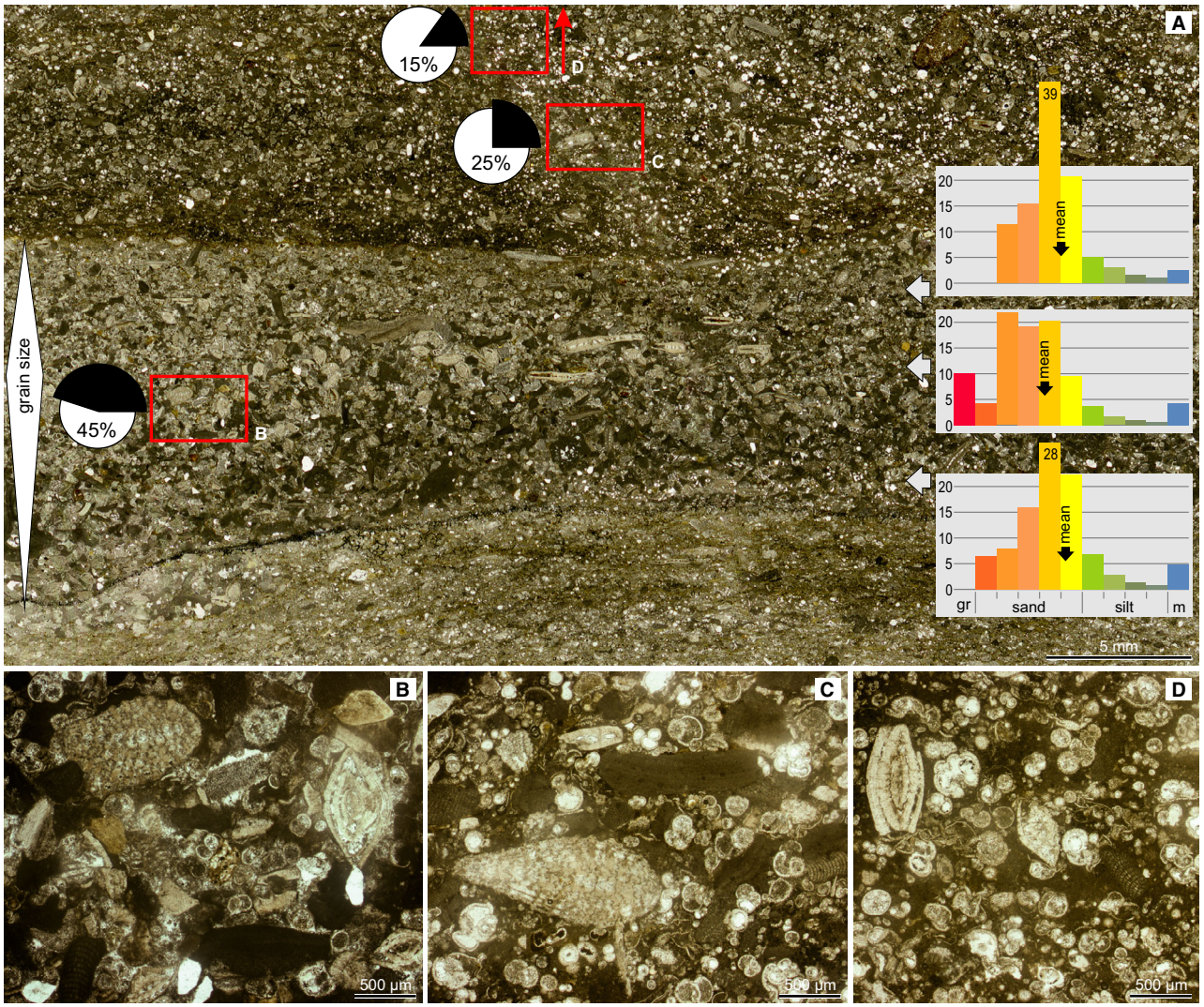

Fig. 10. Microfacies of wavy-layered calcarenites (F3b, globigerinid packstone–grainstone with varying amounts of shallow-water bioclasts) overlying the sharp-based calcirudite bed (F4) in the early Miocene (Pakhna Formation) as part of Petra Tou Romiou section (Samples Pet 2016-2u and 2016-2o). See Fig. 8 for general lithology and sampling points. Interpretation: Bottom-current reworked top of a coarse-grained turbidite. (A) Thin-section scan highlighting compositional change and grain-size variation that are related to the wavy layering (F3b). Layer by layer, the amount of shallow-water bioclastic material decreases upward (see black pie charts). Note inverse to normal compositional grading of the central layer: Corallinacean red algae (dark particles) are more common in the lower part while larger benthic foraminifera prevail in the middle part (bedding-parallel oriented shells of *Heterostegina*). Histograms document mean grain-size shift from very fine sand to medium sand and back to fine sand. Note the granule-sized shells in the middle part. (B) Bioclastic grainstone comprising both shallow-water material (about 45%) (larger benthic foraminifera, corallinacean red algae and crinoids) and planktonic foraminifera (globigerinids). Note the isolated sand-sized quartz grains (white). Thin section Pet 2016-2u. (C) Bioclastic packstone consisting of both larger benthic foraminifera (about 25%) (*Miogypsina*, *Heterostegina* and corallinacean red algae) and planktonic foraminifera (globigerinids). Thin section Pet 2016-2o. (D) Bioclastic packstone–wackestone comprising both shallow-water material (about 15%) (*Amphistegina* and corallinacean red algae) and planktonic foraminifera (globigerinids). Thin section Pet 2016-2u.

This calcarenite facies is formed by globigerinid packstone and grainstone (Figs 12 and 13). Planktonic foraminifera are the main constituent. The fragile tests are mainly well-preserved within the non-compacted layers (Fig. 14A to C, H and I), whereas fragmented

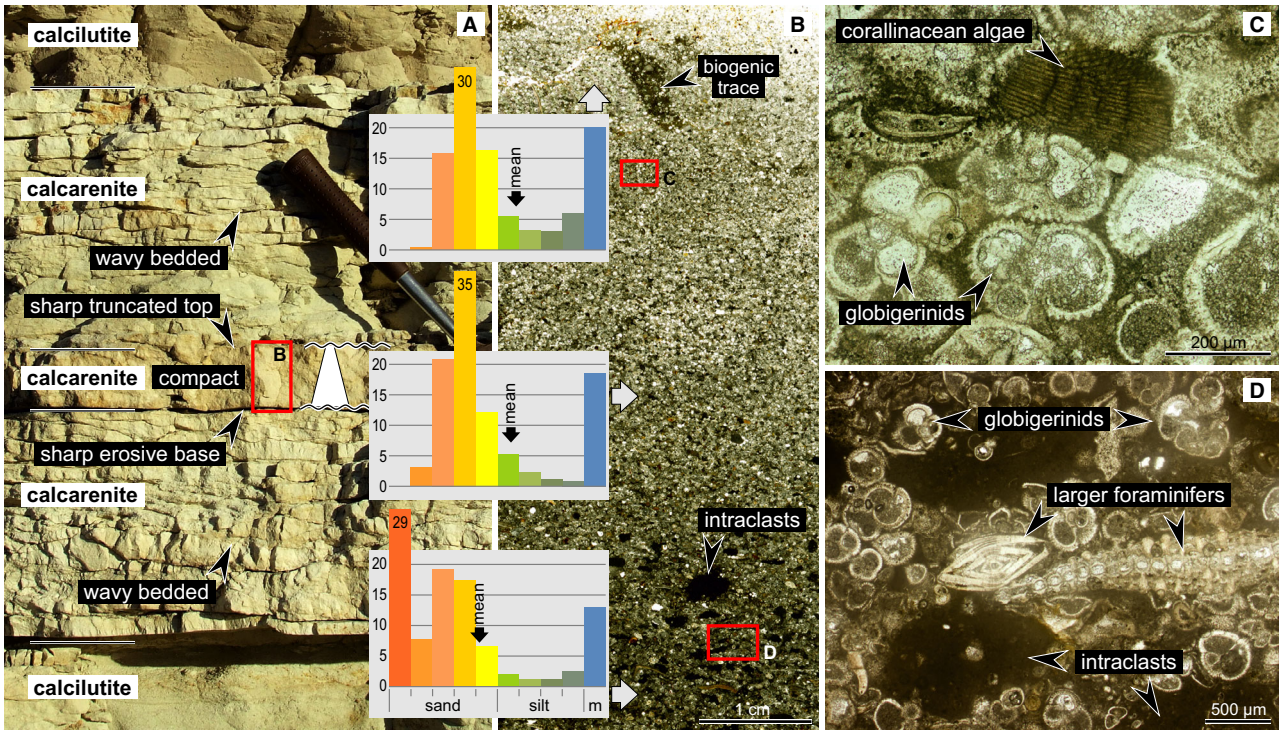

Fig. 11. Calcilutites (F2a, globigerinid wackestone) interstratified with different types of calcarenites. Early to middle Miocene from the Pakhna Formation as part of Petra Tou Romiou section (Sample Pet 74). Interpretation: Fine-grained turbidite (compact bed) embedded within sand-dominated bi-gradational contourite sequences C1–(C2)–C3–(C4)–C5. (A) Photograph showing a sharp-based calcarenite bed with normal grading (F3e, larger-benthic-foraminifera globigerinid packstone) that is embedded within a calcarenite bed with wavy layering (F3b, globigerinid packstone–grainstone with varying amounts of shallow-water bioclasts). Hammer for scale (32 cm long). (B) Thin-section scan of the sharp-based calcarenite bed (F3e). Both the well-developed normal grading and the shallow-water origin of a significant part of the biogenic particles are criteria for a turbidite interpretation. Black particles in the lower part are mainly intraclasts (globigerinid wackestone). Histograms document the decrease of intraclasts and shallow-water bioclasts (very coarse and coarse sand) in favour of globigerinid shells (fine sand) and mud. Note the mean grain-size shift from fine sand to coarse silt. Thin section Pet 74. (C) Bioclastic packstone rich in planktonic foraminifera (globigerinids). Shallow-water material (note, corallinacean red algae) also occurs. (D) Bioclastic packstone comprising planktonic foraminifera (globigerinids), a substantial amount of shallow-water material (larger benthic foraminifera) and intraclasts.

and flattened tests prevail within the compacted layers (Fig. 14D to G). Within the centre of non-compacted layers, the intact globigerinid shells are typically filled with carbonate mud, while they are empty at the lower and upper margin (Fig. 14A to C, H and I). In addition, biogenic activity clearly influenced the preserved fabric. Within parts of the calcarenite beds, both diffuse bioturbational mottling and distinctly-bounded biogenic traces occur.

Although most of the calcarenites are composed entirely of planktonic foraminifera, bioclasts of shallow-water origin are admixed at a certain (usually low) amount within some of the calcarenite beds (Fig. 13). The embedded particles are typically robust skeletons of benthic organisms and derive from shallow-water carbonate environments. Larger benthic foraminifera (*Amphistegina*, *Heterostegina* and *Operculina*), corallinacean red algae, corals, bryozoans, thick-shelled brachiopods and crinoids have been identified. The variety of shallow-water bioclasts is equivalent to the shallow-water particle association of the structureless calcirudite beds (F4). Such shallow-water constituents are particularly common in wavy-layered calcarenites that directly overlie structureless calcirudite beds (Fig. 10). In some cases, however, they also occur in wavy-layered calcarenite beds that are interstratified with whitish and greenish calcilutites (F2a and F2b). It is important to note that the occurrence of shallow-water constituents

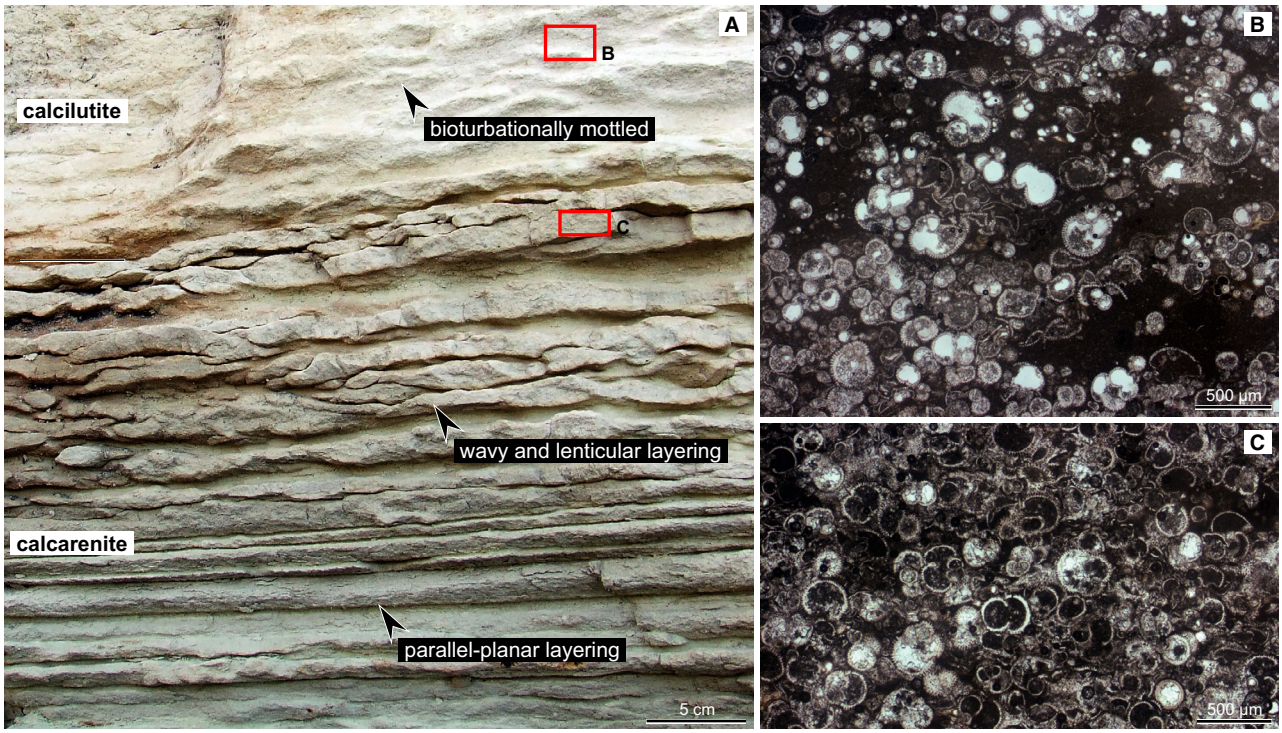

Fig. 12. Greenish calcarenites with internal wavy layering (F3c, globigerinid packstone–grainstone) overlain by whitish calcilutites (F2a, globigerinid wackestone). Early Miocene from the Pakhna Formation as part of Petra Tou Romiou section (Samples Pet 14 and 15). Interpretation: Upper part of a sand-dominated bi-gradational contourite sequence. . . .–C3–(C4)–C5. (A) Outcrop photograph illustrating the variation of the characteristic layering from parallel planar to lenticular and to wavy in the lower and upper part of the calcarenite unit (F3c), respectively. The calcilutite (F2a) appears rather homogeneous. Note the greenish colour in the lower part of the calcarenite, which is caused by higher amounts of illite clays. (B) Bioturbational mottled calcilutite (F2a, globigerinid wackestone–packstone) (Sample Pet 15). (C) Calcarenite (F3c, globigerinid packstone) (Sample Pet 15).

within the wavy-layered calcarenites is not always associated with structureless calcirudite beds (F4) or normally-graded calcarenite beds (F3e), which both are interpreted as shallow-water derived turbidite beds (see below).

The benthic shallow-water bioclasts are evenly distributed among the globigerinid tests, namely a certain amount within each individual calcarenite layer (Figs 10 and 13). This amount changes from layer to layer. In other words, the layering corresponds with a compositional change, which is displayed by a specific ratio between planktonic and benthic (shallow-water) bioclasts. This indicates that the wavy layering has been controlled by a primary sedimentary signal, which is enhanced diagenetically by the formation of non-compacted layers (cementation during early stages of diagenesis) and compacted laminae. Obviously, the non-compacted layers have been lithified by cementation during early stages of diagenesis.

Greenish calcarenite beds with internal wavy layering: globigerinid packstone–grainstone with varying (low) amounts of shallow-water bioclasts and illite (F3c)

Greenish calcarenite beds with wavy layering occur in the upper part of the studied record (Fig. 4). Their microfacies is almost identical with the wavy-layered whitish calcarenites (F3b). In contrast to the latter, however, they are enriched in illite and quartz, with contents of 2 to 3% as indicated by XRD analysis (Hernández-Molina *et al.*, 2018). The fine-grained illite clays are concentrated within the compacted layers together with shale lithoclasts and cause the greenish colouring. Locally, silt-sized and sand-sized quartz grains have been identified in thin sections.

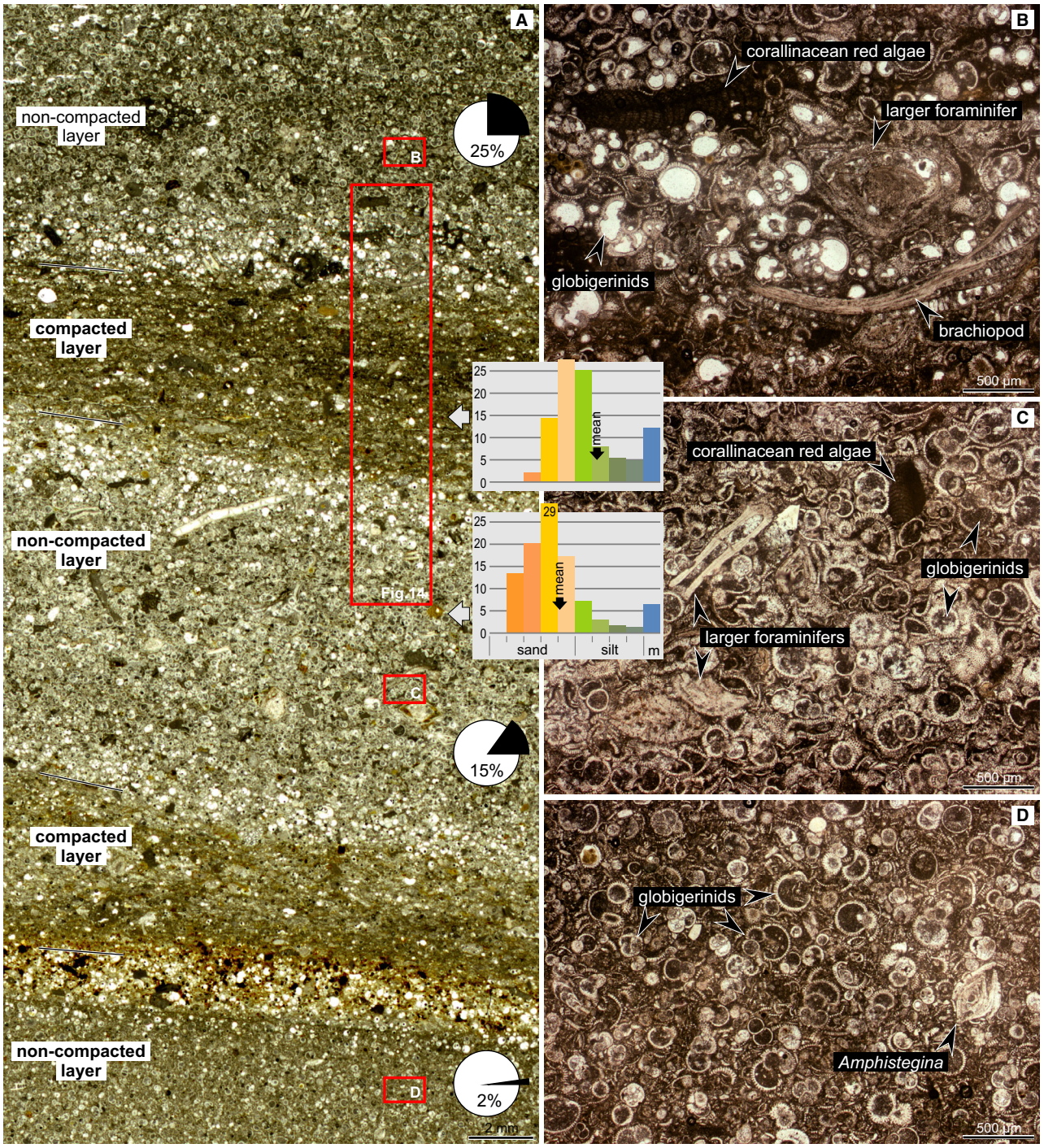

Fig. 13. Microfacies of calcarenite beds with internal wavy layering (F3c, globigerinid packstone–grainstone with varying amounts of shallow-water bioclasts). Interpretation: Calcareous sandy contourite. Early Miocene from the Pakhna Formation as part of Petra Tou Romiou section (Sample Pet 21). See Fig. 4 for general lithology and sampling point. (A) Thin-section scan showing the alternation between non-compacted layers and thinner compacted interlayers that constitute the wavy layering of the calcarenites (F3b and F3c). Note that the amount of shallow-water bioclasts (black portion of pie charts) within the non-compacted layers is layer specific. Note histograms that exemplify variation in grain size between non-compacted layers and compacted layers. (B) 25% shallow-water bioclasts occur among globigerinids. (C) 15% shallow-water bioclasts (larger benthic foraminifera and corallinacean red algae) occur among globigerinids. (D) 2% shallow-water bioclasts (*Amphistegina*) occur among globigerinids.

SEDIMENTARY FACIES INTERPRETATION

Pelagic deposits

Pelagic carbonate muds, formed by the continuous rain of calcareous planktonic skeletons to the seafloor in deep-marine environments, represent the autochthonous background facies within the studied record. These sediments are identified as mottled calcilutite beds consisting of bioturbationally churned globigerinid wackestone (F2a), with no evidence of current-controlled deposition. The trace fossil assemblage, assigned to the *Zoophycos* ichnofacies, supports the pelagic character (Miguez-Salas & Rodríguez-Tovar, 2019a). Those pelagites constitute most of the Eocene part of the section. Where calcilutites form thin interbeds between thicker calcarenite beds within the early and middle Miocene part of the section, they may also represent pelagic carbonates. Where calcilutites are part of bi-gradational cycles together with thicker wavy-layered calcarenite beds (F3b and F3c); however, they may also signify muddy contourites resulting from remobilized pelagic mud under conditions of weak bottom currents (see below).

Muddy contourites (contourite divisions C1 and C5)

Muddy contourites, which result from deposition of fines directly from suspension through a laminar boundary layer, are generally homogeneous and highly bioturbated, often with an indistinct mottled appearance (as described by Gonthier *et al.*, 1984, and Stow *et al.*, 2008). Therefore, both the whitish and the greenish calcilutites (F2a and F2b) are interpreted as muddy contourites (for example, Figs 3, 4, 5C, and 5D). Fabrics are bimodally sorted. Micrite is the predominant mode (*ca* 75%) while globigerinids form a subordinate discrete mode (*ca* 25%) with a maximum at very fine sand. The mean grain size is fine silt (Figs 5B and 6B). McCave & Hall (2006) calculate that such mud-dominated calcareous contourites with a low content of foraminiferal tests are deposited at current speeds <20 cm s^{-1} mainly by selective deposition from the nepheloid layer.

The whitish calcilutites (F2a), which form thick structureless beds and bedsets within the Eocene part of the section, show in some cases decimetre-scale banding marked by subtle colour changes, as is typical for muddy contourites. Based on microfacies characteristics, the source area of the muddy calcareous contourites can be attributed to a deep-water pelagic environment. Weak bottom currents have intercepted sinking planktonic material and/or have eroded pelagic calcareous ooze since nannofossil mud and well-preserved globigerinids tests are the only characteristic constituents.

Many of the calcilutite interbeds within the early and middle Miocene part of the section (and even some calcarenite beds) exhibit a greenish colour (F2b), which results from enrichment in illite (and quartz) up to 3% (Hernández-Molina *et al.*, 2018). These siliciclastic admixtures may be caused by bottom-current controlled sediment entrainment from siliciclastic sources (see He *et al.*, 2008; Stow & Faugères, 2008) or by hemipelagic advection of fine-grained materials within the water column (see Henrich & Hüneke, 2011). Thus, the greenish calcilutite facies (F2b) may represent muddy contourites or hemipelagic deposits (see below). The Troodos ophiolite complex, which has been already subject to uplift and alteration during the formation of the studied record (Eaton & Robertson, 1993), represents a potential source area for very fine-grained sediments which could be transported basinward for long distances as sediment in suspension through nepheloid layers.

Silty contourites (contourite divisions C2 and C4)

Calcisiltites *sensu stricto*, i.e. sediments composed to a large extent of silt-sized particles, form thin interlayers within the wavy-layered calcarenite beds of facies F3b and F3c (Figs 4 and 13). These interlayers of micro-bioclastic packstone are essentially made of heavily fragmented globigerinid shells (Fig. 14A and D to G). In addition, some of the documented coarser-grained facies can be compared with calcisiltites. Layers of globigerinid packstone with a groundmass of carbonate mud (equivalent to packed biomicrites), which are a substantial part of facies F3a and F3b, have an average grain size of silt (Figs 5 and 6). This mean grain size results from the bimodal composition of this depositional texture: Globigerinids are well-preserved in most of the facies and constitute the arenitic (sand-sized) particles (occasionally together with the shallow-water materials), while the lutitic particles (carbonate mud) are mainly provided

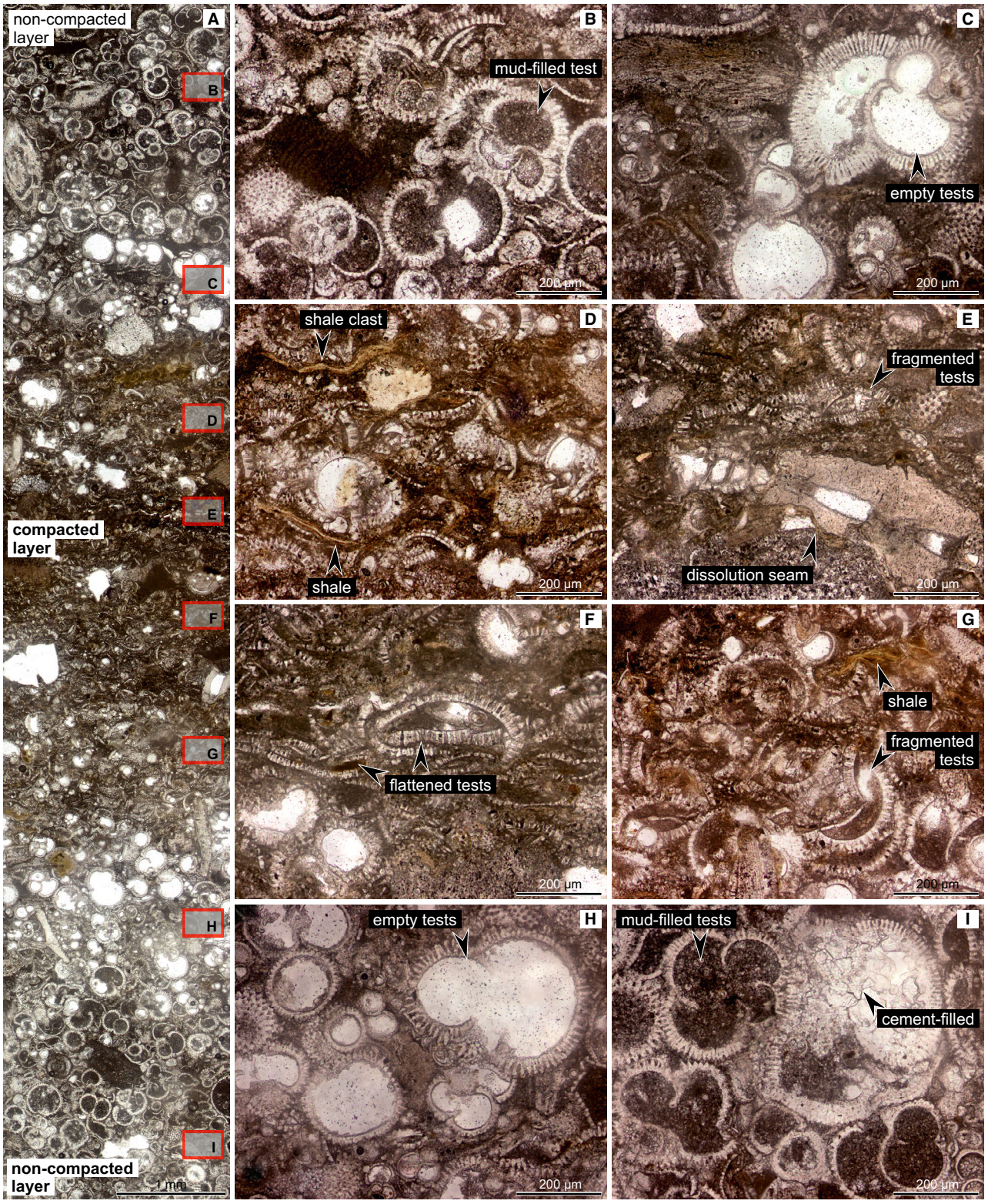

by nannoplankton (coccolithophorids). Such mud-rich calcarenites may be classified as silty contourite divisions (C2 and C4).

Within the studied record of Cyprus, however, calcisiltites rarely form distinct C2 and C4 contourite divisions. This is a clear difference

Fig. 14. Microfacies and diagenetic features of calcarenite beds with internal wavy layering (F3c, globigerinid packstone–grainstone with varying amounts of shallow-water bioclasts). See Fig. 13 for sampling point (Sample Pet 21). (A) Microphotograph showing change of depositional texture from non-compacted to compacted layers and vice versa. Interpretation: Lamina sets of intact-mud-filled, intact-empty, and fragmented globigerinid tests reflect decreasing flow speed and vice versa increasing flow speed. (B) The ubiquitous globigerinids are largely intact and mud-filled within the non-compacted calcarenite layers. (C) Intact but empty globigerinid shells predominate at the lower margin. (D) Fragmented globigerinid shells and shale lithoclasts, which were deformed due to compaction, characterize compacted layer. (E) Fitted fabric due to compaction and pressure dissolution along grain boundaries. (F) Collapsed and flattened globigerinid shells resulting from compaction. (G) Compacted shale lithoclast among highly fragmented globigerinid shells. (H) Intact globigerinids are mainly empty at the upper margin of the non-compacted layer. (I) Whole, mud-filled and some cement-filled globigerinid shells mainly constitute the compacted layer.

compared with modern counterparts of mixed siliciclastic/bioclastic composition (Gonthier *et al.*, 1984; Stow & Faugères, 2008; Brackenridge *et al.*, 2018) and the Devonian calcareous contourites in Europe and northern Africa documented by Hüneke (2007, 2013), in which calcisiltites of fragmented skeletal elements are widespread and are deposited in thin but discrete beds with faint normal and inverse grading. The scarcity of calcareous silt within the Eocene–Miocene contourites is subject to two conditions: First, the sediments reworked by bottom-current activity within the source area were obviously devoid of silt-sized bioclasts. This is an archetypical feature of pelagic carbonates, which characteristically show bimodal grain-size distribution with a general minimum between 4 μm and 16 μm (see Flügel, 2010; Frenz *et al.*, 2005). This minimum defines the transition of foraminifer and coccolith

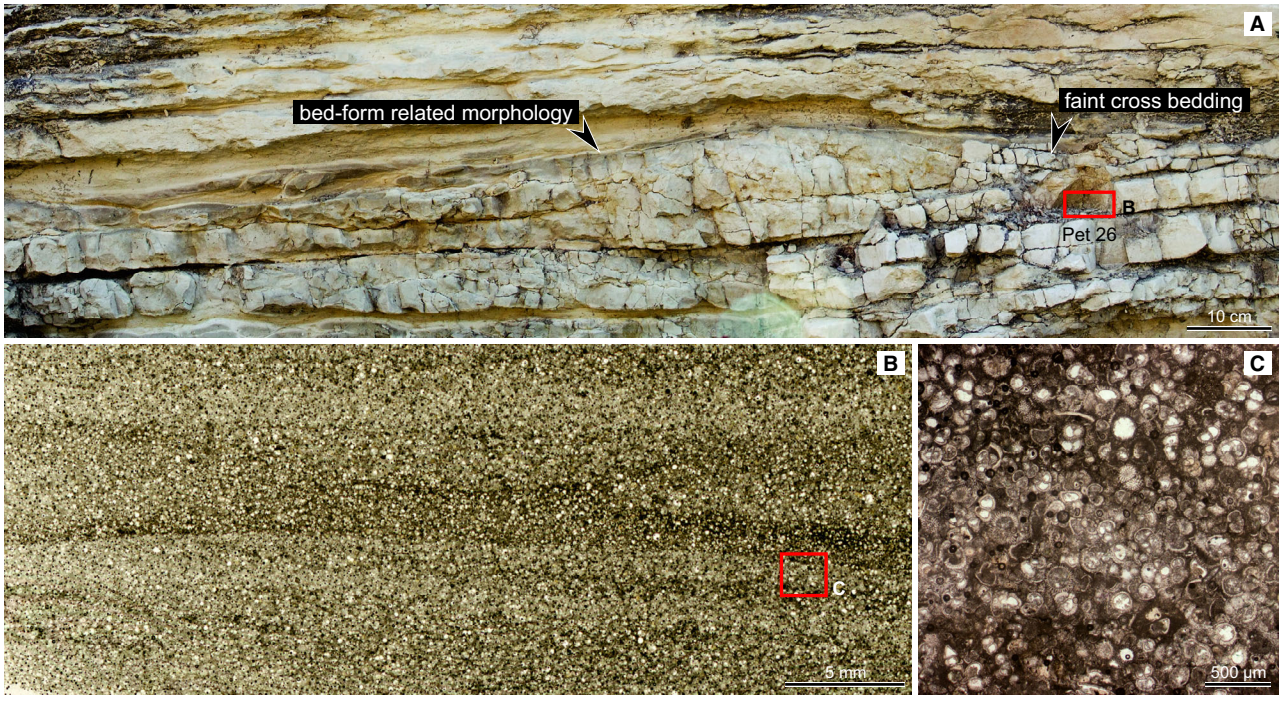

Fig. 15. Calcarenites with internal wavy layering (F3b, globigerinid packstone–grainstone). Interpretation: Calcareous sandy contourite. Early Miocene from the Pakhna Formation as part of Petra Tou Romiou section (Sample Pet 26). (A) Outcrop photograph of a calcarenite bed (F3b) that preserves a bed-form-related upper boundary (mega ripple, subaqueous dune) and relic cross-bedding. (B) Thin-section scan of the calcarenite bed (globigerinid packstone) illustrating local well-preserved cross-lamination (F3b). (C) Microphotograph illustrating the particle-supported texture of the sorted globigerinid packstone (F3b).

carbonate. Within the pelagic carbonate factory, organisms that produced skeletons of silt size in significant quantities are the exception. Moreover, mechanical disintegration of sand-sized globigerinid shells into silt-sized fragments during transport within the bottom current was minimal at current speeds up to 20 cm s^{-1}, which typically control the accumulation of silty contourites (McCave & Hall, 2006; McCave, 2008). Consequently, distinct calcisiltite divisions are rarely part of the contourite depositional sequences.

Within the wavy-layered calcarenite beds (F3b and F3c), the micro-bioclastic debris of the interlayers is of fine sand to coarse silt size (mean: coarse silt) and largely results from fragmentation of the fragile globigerinid tests (Fig. 14A and D to G), whereby the skeletal breakdown was increased – at least partially – by diagenetic compaction (Fig. 14E and F). These interlayers show that the fragmentation of globigerinid tests is more closely related to the accumulation of calcarenite beds (see *Sandy contourites* section below) and thus to current speeds above 20 cm s^{-1}, which favour accumulation of foraminiferal sand (McCave & Hall, 2006; McCave, 2008). Such extensive shell fragmentation under conditions of increased hydrodynamic agitation is known as textural inversion and is a specific feature of bioclastic sediment accumulation (Folk, 1962; Flügel, 2010).

Sandy contourites (contourite division C3)

Thin irregular calcarenite beds (F3a) occur within the Eocene part of the studied record (Fig. 6), while thick calcarenite beds and bed sets with wavy layering (F3b and F3c) prevail within the early and middle Miocene part of the record (Figs 3, 4, 12, 13 and 15).

Thin calcarenite beds

The thin calcarenite beds with gradational boundaries (F3a), consisting of globigerinid wackestone–packstone, are best interpreted as bioclastic (fine-grained) sandy contourites (Fig. 6). The weak bottom-current induced enrichment of foraminiferal tests over carbonate mud gave way to thin foraminiferal sand sheets with local particle support. A bimodal grain-size distribution is characteristic. Within thin calcarenite beds, globigerinids form a discrete mode (*ca* 50%) with a maximum of fine sand (Figs 5B and 6B). In addition, micrite is omnipresent (*ca* 50%). However, the latter may represent a subsequent infill due to decreasing flow velocity and bioturbation. They are most probably formed by selective deposition of particles released from the nepheloid layer on the basis of settling velocity through the boundary layer (see McCave & Hall, 2006; McCave, 2008). McCave & Hall (2006) calculated that such contourite sands rich in interstitial mud will be formed at current speeds between 20 cm s^{-1} and 30 cm s^{-1}. Selective erosion of the carbonate mud (winnowing) has probably not been an important bottom-current induced sorting process, because fine-grained sediments, even calcareous muds, behave cohesively and are subject to particle aggregation (Winterwerp & Van Kesteren, 2004; McCave, 2008).

It is difficult to differentiate between the two modes of sorting (enrichment of foraminifera) by means of microfacies, since most depositional structures were severely degraded by biological disturbance. Winnowing of carbonate mud may have been at least an additional sorting process, since some of the thin calcarenite beds with gradational boundaries (F3a) pinch out laterally over a distance of several metres and pass over into erosional surfaces, as indicated by the ichnological features (Rodríguez-Tovar *et al.*, 2019a). Winnowing can make a calcarenite deposit somewhat coarser overall by producing intermittent erosion horizons marked by coarse silty and sandy lags (McCave & Hall, 2006; Castro *et al.*, 2020). Net removal of fines by winnowing starts at flow speeds between 20 cm s^{-1} and 25 cm s^{-1} (Miller & Komar, 1977). Higher current speeds are critical for the movement of foraminifera.

The faint lamination locally preserved represents relic structures from bedload transport or from current shear. In most cases, however, the impact of diagenetic pressure dissolution is intensive and obscured most of the primary tractional structures. The particle composition – exclusively shells of calcareous plankton – indicates bottom-current induced reworking of pelagic carbonate muds within the source area or *in situ*.

Together with the underlying and overlying strata, the thin calcarenite beds are part of bigradational calcilutite–calcarenite–calcilutite sequences (Figs 5 and 6). Complete cycles of mean grain size and depositional texture include coarsening-upward sequences (from globigerinid wackestone to globigerinid packstone) and fining-upward sequences (from globigerinid packstone to globigerinid wackestone), which can be

related to the standard sequence of facies by Gonthier *et al.* (1984) and Stow & Faugères (2008) for contourites in relation with increasing and decreasing bottom-current velocities, respectively.

Thick calcarenite beds with internal wavy layering

Whitish and greenish calcarenites with internal wavy layering (F3b and F3c) form thick beds and bed sets of bioclastic sandy contourites (Figs 3, 4 and 12). These consist of globigerinid packstone–grainstone showing clear particle support and a (varying) low mud content as a result of sorting during bottom-current induced sediment transport and deposition (Fig. 13). The locally well-preserved parallel and cross-lamination is indicative of bed-load transport (Fig. 15). Nevertheless, the non-compacted layers of such thicker calcarenite beds are mainly bimodally sorted (Figs 13 and 14). Polymodal sorting occurs in layers where shallow-water particles are common (above coarser-grained turbidites, F4) (Fig. 10). The prevalent globigerinids form a discrete mode (>70%) around fine-grained sand (Figs 10A and 13A). Micrite is less omnipresent (<10%). Mean grain size varies between fine and very fine sand.

Although particle sorting by bottom currents typically occurs by selective deposition, winnowing of carbonate mud occurs in addition under conditions of stronger flows where the currents frequently exceed *ca* 20 cm s^{-1} (McCave, 2008). Between 20 cm s^{-1} and 30 cm s^{-1}, clay particles and carbonate mud are increasingly removed, finally giving way to a well-washed sandy lags (McCave & Hall, 2006). Modern analogues are the foraminiferal sands of equatorial and mid-latitudes with a particle density of 1.1 to 1.5 g cm^{-3} for medium-sized tests (Miller & Komar, 1977) and the Gulf of Cadiz (Sierro *et al.*, 1999). Although such foraminifera have the erodibility of very coarse silt, they have the settling velocity of very fine sand and are not transported over great distances, being largely confined to bedload (McCave, 2008). At current speeds above 30 cm s^{-1}, foraminiferal sand will be sufficiently mobile to contain little mud and able to form ripples and small sandy dunes (Stow *et al.*, 2009).

The authors interpret the wavy layering (and the more rarely occurring lenticular or planar layering) as a primary sedimentary feature (Figs 4 and 12), whereas diagenetic change is identified as a secondary modifying process. The layer-specific amount of benthic shallow-water bioclasts is the main argument (Fig. 13). This interpretation is confirmed by the rarely preserved parallel and cross-lamination, forming laminae sets within the non-compacted layers (Fig. 15). Both the calcarenite layers and the finer-grained interlayers have been modified by bioturbation and, subsequently, to some degree by diagenetic processes (Figs 14 and 16). Due to differential cementation, the internal wavy layers have been cemented during early stages of diagenesis, while compaction mainly affected the intervening clay-containing interlayers.

The wavy layering is interpreted to represent a discontinuous accumulation of sandy lags and individual ripple trains that migrated episodically over the seabed leaving behind laminasets of parallel-laminated and cross-laminated calcarenites (Fig. 16). These rather short-lived depositional events from foraminiferal bedload transport (current speeds around 30 cm s^{-1}), which produced individual calcarenite layers (sediment-filled and empty globigerinids), alternated with longer periods of intensified suspension settling (current speeds around 20 cm s^{-1}), which formed the finer-grained interlayers of fragmented globigerinids (Figs 13 and 14). The fine sand-sized to coarse silt-sized shell fragments have been transported in the lower part of the turbulent boundary layer and are deposited first when the bedload stops moving (see McCave, 2008). This interpretation of current velocities considers both the different grain-size of whole and fragmented globigerinids and the variable bulk density of sediment-filled (*ca* 2.71 g cm^{-3}) and empty (1.2 to 1.5 g cm^{-3}) globigerinid shells (Fig. 14). Furthermore, sediment bypassing and non-deposition together with intensified shell fragmentation (textural inversion) may have occurred at still higher current speeds (above 40 cm s^{-1}). Under such conditions, near-seafloor cementation rates may increase (Mullins *et al.*, 1980; Eberli & Betzler, 2019; Mulder *et al.*, 2019). Subsequent bioturbation and the diagenetic processes described above are responsible for obscuring and alteration of these primary sedimentary structures.

The **source area** of the sandy contourites (F3a, F3b and F3c) can be attributed to a deep-water pelagic environment. Bottom currents have redistributed mainly pelagic calcareous ooze since well-preserved globigerinid tests are the main sand-sized constituents (Figs 6 and 12). In addition, a few calcareous turbidites have been reworked, which have had the same neritic

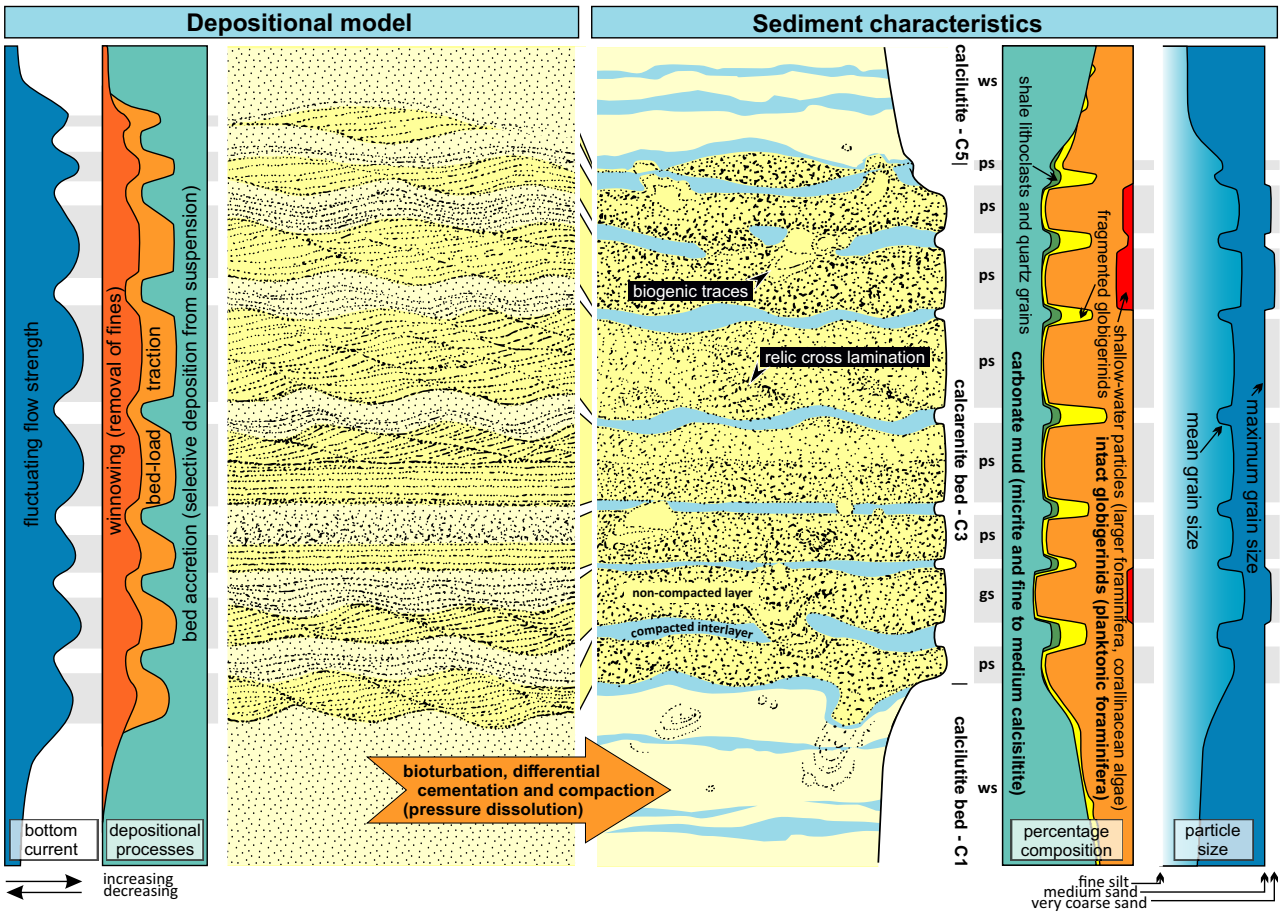

Fig. 16. Sediment characteristics of the calcareous sandy contourites from the early and middle Miocene (Pakhna Formation) at Petra Tou Romiou on Cyprus. The entire coarsening-upward to fining-upward sequence is thought to have been deposited from a bottom current, whose flow strength rhythmically fluctuated. The interbedding of calcilutites (F2a and F2b) and calcarenites (F3b and F3c) is produced by long-term fluctuation (contourite divisions C1–C3–C5), whereas the wavy layering of the calcarenite beds (F3b and F3c) results from short-term fluctuations (contourite division C3). Phases of flow acceleration caused the recurrence of rippled-bed traction (temporary plane-bed transport?). Phases of flow deceleration caused dumping of sediment suspension, effectively suppressing traction and inducing bed accretion (draped lamination and normal grading). Changes in percentage composition and grain-size are shown schematically based on visual estimation. Note that the mean grain size of the calcarenites is mainly determined by the ratio of carbonate mud (plus clay) versus globigerinids (plus shallow-water material). This is due to the bimodal sorting that packstone and wackestone layers inevitably show. The maximum grain size is defined and limited by the size of the globigerinid test (medium sand) or by the shallow-water calcareous detritus (typically very coarse sand). The latter occur in some individual layers only. The more fine-grained (clay-rich) layers are prone to chemical compaction by pressure dissolution and gave way to the formation of dissolutions seams (= compacted interlayers). Coarse-grained (well-sorted) calcarenite layers have been cemented during early diagenesis and are not compacted (= non-compacted layers). Abbreviations: ws = wackestone, ps = packstone, gs = grainstone; C1, C2, C3 = contourite divisions.

particle composition as the turbidites documented from the Petra Tou Romiou section (F3e and F4). The shallow-water bioclasts were embedded in lower quantities among the prevailing planktonic globigerinids only within some layers of the calcarenite beds with wavy layering (F3b and F3c) (Figs 4 and 13). They are different in shape, composition and density, so they often form outsized clasts and do not display grading properly (Figs 13 and 14), which is a carbonate-specific feature (Eberli & Betzler, 2019). Layers with frequent shallow-water particles, however, nicely reveal inverse and normal grading (Fig. 10). The siliciclastic admixtures of

illite and silt-sized shale lithoclasts (plus quartz particles) within the greenish calcarenites with internal wavy layering (F3c) (Fig. 4) indicate bottom-current controlled sediment entrainment from siliciclastic sources (see He *et al.*, 2008; Stow & Faugères, 2008; Mulder *et al.*, 2013). The Troodos ophiolite complex, which has been already subject to uplift and alteration during the Oligocene–Miocene (Eaton & Robertson, 1993), represents a potential source area.

Fine-grained turbidites

Fine-grained turbidites are recognized in all parts of the section (F3d and F3e). They form beds less than 10 cm thick within the lower (Eocene) part (F3d) and up to 20 cm thick within the upper part of the studied record (early and middle Miocene) (F3e). They can be discriminated by means of a sharp (erosional) base, (indistinct) normal grading, and in many cases a well-developed lamination (at least within the lower part of a bed) (Figs 6 and 7). Although the upper boundary is essentially gradational, it may also show more abrupt changes in grain size or even local reworking. The latter may be caused by hydraulic reworking or biogenic activity (or both) controlled by bottom-current activity (see Mulder *et al.*, 2008).

In most cases, such calcarenite beds show bimodal sorting characterized by a discrete mode around fine sand of globigerinid shells (Figs 7B and 11B). In addition, micrite is omnipresent, constituting a subordinate mode at the base and a dominant mode at the bioturbated top of the bed (Fig. 7B). Polymodal sorting occurs, where intraclasts and shallow-water particles are involved (Fig. 11B).

The thin sharp-based calcarenite beds consisting of globigerinid packstone–grainstone (F3d) can be interpreted as fine-grained (distal) turbidites with bioturbated tops. The pelagic-sediment provenance indicates supply from deep-marine slope settings or adjacent pelagic highs (Fig. 7). Since these beds do not comprise bioclastic shallow-water detritus, the density flows must have been supplied from a setting of pelagic calcareous oozes.

Some of these turbidites were affected by bottom currents after their deposition, since they show signs of reworking at the top or even complete reworking of the whole bed. Complete reworking can be recognized by lateral thinning out of the bed over a distance of several metres up to tens of metres and transition into an irregular layer interface, which is in many cases diagenetically enhanced by pressure dissolution. Remnants of those locally eroded turbidite beds are preserved in burrow fills below the erosional surface (see Rodríguez-Tovar *et al.*, 2019a).

The sharp-based calcarenite beds with normal grading consisting of larger-benthic-foraminifera globigerinid packstone (F3e) are interpreted as turbidites derived from shallow-water depositional environments (Fig. 11B). The benthic particle association, including larger foraminifera (*Amphistegina*, *Heterostegina* and *Operculina*) and corallinacean algae, indicate a euphotic source area of an open carbonate platform (see Beavington-Penney & Racey, 2004), equivalent or probably identical to the Terra Member (Fig. 11C and D). Normal grading and particle composition reveal fully turbulent flows that have been enriched with planktonic material (globigerinids) due to erosion under waxing-flow conditions across the slope. Erosion can also be inferred from the presence of rip-up clasts in the sequence or clasts collapsed from undercut banks. Alternatively, these turbidites may have been supplied from outer shelf settings or from a slope terrace hosting both shallow-water benthic and open-ocean planktonic materials. Such a source area could be described as a transfer region, accommodating both carbonate-platform debris and pelagic rain, and would also explain the balanced ratio of neritic and pelagic bioclasts of the F3e-facies turbidites.

Sharp, irregular and truncated upper boundaries may signify turbidite beds that have been reworked after deposition under the control of concurrent bottom-current activity (see Lee & Ogawa, 1998; Ito, 2002; Gong *et al.*, 2016). As a result, confirmed by the documented microfacies, shallow-water particles became remobilized and admixed into the overlying calcarenite layers interpreted as contourites (F3b and F3c).

Coarser-grained turbidites

Thick calcirudite beds (up to 50 cm) consisting of predominant shallow-water bioclastic materials (Figs 8, 9 and 11) represent coarser-grained turbidites (F4), and occur within the early and middle Miocene part of the studied record. They display a sharp (erosional) base. Lamination or normal grading may be indistinct, if developed at all, as is typical for calcareous turbidites composed of bioclasts with varying specific weights and polymodal grain-size populations (grain size is controlled by skeletal producers).

The sharp-based calcirudite beds consisting of larger-benthic-foraminifera corallinacean rudstone

(F4) are turbidites that have been supplied from shallow-marine sources (Fig. 9). Larger benthic foraminifera and corallinacean calcareous red algae indicate a euphotic source area such as represented by the Terra Member. The association of *Amphistegina*, *Heterostegina* and *Operculina* suggests supply from an open carbonate ramp or reef foreslope within the deeper euphotic zone between 40 m and 120 m (Beavington-Penney & Racey, 2004). The responsible density flows must have had some erosive capacity, since individual globigerinids and intraclasts, consisting of globigerinid wackestone and globigerinid packstone, have been incorporated from the seabed. This is supported by the sharp and locally truncating basal contact of the beds.

The indistinct basal grading of the calcirudite beds suggests that turbulence and suspension fallout had no time to occur (because of high particle concentration or due to the coarse particle size). Thus, these turbidites can be interpreted as a concentrated-flow deposit (see Mulder & Alexander, 2001; Mulder, 2011). This interpretation is treated with caution, however, since the bioclastic grains are different in shape, composition and bulk density. The relation between particle size and flow behaviour is therefore not as straightforward as it is in siliciclastics (Eberli, 1991; McCave & Hall, 2006; Eberli & Betzler, 2019).

Turbidite beds may show gradual upper boundaries that reflect deceleration of the density flow and fine-particle fallout from the turbulent tail of the flow. The sharp upper boundaries of the calcirudite beds of facies F4 may indicate turbidites that have been reworked after deposition by bottom-current activity (Fig. 8). Reworked turbidite tops are the result of such winnowing processes (Fig. 10). In addition, shallow-water bioclastic particles have been admixed into the bottom boundary layer, which is otherwise dominated by material from pelagic sources, and became redistributed by the bottom currents. As a result, contourites formed above and leeward of such reworked turbidites include a significant amount of shallow-water bioclasts (see F3b and F3c) (Figs 10 and 13).

DISCUSSION

Sequences of contourite facies

Bottom-current induced sedimentation is documented by interbedded calcareous muddy contourites (calcilutites) and calcareous sandy contourites (calcarenites).

Association of facies

All facies interpreted as sandy contourites **(F3a, F3b and F3c)** are associated with whitish or greenish calcilutites (F2a and F2b), which are interpreted as muddy contourites (F2a and F2b) or pelagic carbonate muds (F2a), respectively. Together with these underlying and overlying beds, they form bi-gradational calcilutite–calcarenite–calcilutite cycles that are comparable with the standard contourites sequence (Figs 3, 5 and 6). These bi-gradational sequences can be causally linked, either to long-term variation in bottom-current velocity, or to temporal variation in local sediment supply (Gonthier *et al.*, 1984; Stow *et al.*, 1986; Stow & Faugères, 2008).

Indistinct boundaries between calcilutites and calcarenites signify a gradual change in depositional regime or may result from biogenic activity. Both a gradual change in bottom-current velocity and a shifting intensity of burrowing or seabed colonization may be involved. The effect of biogenic activity is limited, however, since the wavy layering is an omnipresent feature.

More distinct, sometimes sharp, boundaries at the base of wavy-layered sandy contourites (**F3b and F3c**) typically occur where calcirudite beds (F4) have been truncated (Figs 8 and 10). Such top-winnowed and reworked calcareous turbidites are the source of shallow-water bioclasts (larger foraminifera, corallinacean red algae, etc.). Density flows have carried most of the shallow-water skeletal elements to slope settings of Cyprus, where such particles have been affected by contour currents of sufficient energy to induce the reworking process. In other cases, a complete reworking of calcareous turbidites must have led to complete recycling and redistribution of shallow-water materials by bottom-currents, since such materials are admixed at significant quantities in many calcarenite contourite beds that form bi-gradational sequences with calcilutites (and show gradual boundaries). In these cases, they are not associated with underlying turbidite beds (Figs 4 and 13).

Mud-dominated contourite sequences. Within the Eocene part of the record, thick calcilutite beds (F2a) together with thin calcarenite beds (F3a) form bi-gradational grain-size cycles (coarsening-upward to fining-upward) (Figs 5 and 6). They are interpreted as bottom-current controlled in origin. Change in mean grain size

and depositional texture (mud-supported → particle-supported → mud-supported) is distinctly gradual, as is characteristic for contourites (Stow & Faugères, 2008). Although the calcilutites related to these cycles represent obviously muddy contourites, their delimitation from pelagic deposits is arbitrary (see *Pelagic deposits* section), in particular with increasing distance from calcarenite beds.

The coarsening-upward to fining-upward sequences are described using the contourite divisions C1–(C2)–C3–(C4)–C5 from Stow & Faugères (2008) (Figs 5 and 6). In cases were the coarsening-upward is reflected by increasing packing density (from sparse to packed biomicrites) but does not culminate in clear particle-support (poorly washed biosparite), the contourite divisions C1–(C2)–(C4)–C5 can be used. The C2 and C4 divisions are indicated in brackets, since bimodally sorted carbonates of wackestone–packstone with a mean grain size of silt do not represent calcisiltites *sensu stricto* (see *Silty contourites* section). Genuine calcisiltites do not form separate divisions within the mud-dominated contourite sequence. Therefore, the boundaries between the divisions are more pronounced than in siliciclastic counterparts, which show complete grain-size distributions.

Sand-dominated contourite sequences. Thick whitish and greenish calcarenite beds with wavy layering (F3b and F3c) prevail within the early and middle Miocene part of the record. They form together with whitish and greenish calcilutite beds (F2a and F2b) bi-gradational grain-size cycles (coarsening-upward to fining-upward). In addition, thin calcarenite beds (F3a) occur. Typical facies sequences are F2a–F3c–F2a (Figs 4 and 12), F2b–F3b–F2b and F2b–F3c–F2b (Fig. 3). They all are interpreted as of bottom-current controlled origin and related to *long-term fluctuations of the flow strength or sediment supply*. In modern contourite drifts characterized by a compositional siliciclastic–bioclastic mixing (*sensu* Chiarella *et al.*, 2017), such stacked sequences indicate cyclic variation in the forcing variables with periodicities between 3000 years to 10 000 years (Brackenridge *et al.*, 2018). The prominent changes in mean grain size and depositional texture (mud-supported → particle-supported → mud-supported) in the calcicontourites within the upper part of this studied section appear to be less gradational than those of the standard model for mixed contourite sequences (see *Mud-dominated contourite sequences* section). The boundaries are rather distinct (Figs 4 and 12); locally sharp, within some of the cycles (Fig. 11). They are, however, never erosional. The interbedded calcilutite beds are typically thinner than the calcarenite beds and represent muddy contourites rather than pelagic deposits.

The coarsening-upward to fining-upward sequences are described using the contourite divisions C1–(C2)–C3–(C4)–C5 from Stow & Faugères (2008) (Figs 3, 4 and 12). The brackets indicate that bimodally sorted carbonates of wackestone–packstone with a mean grain size of silt form the C2 and C4 divisions within the contourite sequence instead of calcisiltites *sensu stricto* (see *Silty contourites* section). The hydrodynamic interpretation of the grain-size related depositional cycles must consider the low bulk density of sediment-filled and empty globigerinid tests (McCave, 2008). Berger & Piper (1972) have experimentally determined settling velocities of empty tests of modern planktonic foraminifera. The settling velocity of a globular shell is equivalent to that of a quartz sphere of diameter approximately 2.4 times less than the maximum diameter of the foraminifer, whereby large variations from this mode occur and result from varying test shapes and wall thicknesses. Thus, the divisions of globigerinid packstone and grainstone, which typically show a grain size of medium sand, represent redistributed sediments that behaved as very fine-grained quartz sand. Consequently, the rapid grain-size shifts from muddy (C1) to sandy (C3) and back to muddy (C5) contourites are less significant from a hydrodynamic point of view.

A specific feature of the thick sandy contourites (C3) within the early and middle Miocene part of the record is the **wavy layering** preserved in calcarenite beds of facies F3b and F3c, which shows transitions vertically into lenticular, flaser and parallel layering (Figs 4 and 12). It can be described as a heterolithic fabric, since the compacted interlayers reflect a higher primary proportion of finer-grained particles (fragmented globigerinids and shale lithoclasts) compared to the cemented layers (Figs 13 and 14). The authors interpret this characteristic as resulting from a repeated change between bedload deposition and increased suspension fallout (Fig. 16). This alternation thus represents relatively *short-term fluctuations of the flow strength* of a deep-marine bottom current. The migration of ripple trains would have been regularly intermittent and/or modified by sediment

fall-out through the bottom-boundary layer. The primary sedimentary succession (before onset of bioturbation, compaction and cementation) is thought to have been that of cross-laminated and parallel-laminated calcarenite layers interbedded with slightly finer-grained (calcarenite–)calcilutite interlayers showing draped lamination and normal grading (Fig. 16). Similar facies have been described recently in sandy contourites of the Gulf of Cadiz (Castro *et al.*, 2020).

Based on ichnological investigations, Rodríguez-Tovar *et al.* (2019b) provided independent evidence for primary compositional differences between the cemented (non-compacted) and the compacted layers. The record of trace fossils (*Chondrites* and *Planolites*) and its peculiarities indicate repetitive episodes of reduced sediment accumulation (or even non-deposition) associated with regular changes in substrate consistency during formation of the calcarenite beds (division C3).

Thus, short-term fluctuations in flow strength evidently induced regular changes in depositional processes during the accumulation of thicker calcarenite beds. Phases of flow acceleration caused the recurrence of bed-load traction. Both rippled-bed traction (Figs 4 and 12) and local plane-bed transport occurred (Fig. 12). More rarely, subaqueous dunes have been formed (Fig. 15). Phases of flow deceleration caused dumping of sediment suspension, effectively suppressing traction, giving way to draped lamination and grading. Deceleration pulses in some cases changed plane-bed transport to ripple-bed transport, showing uninterrupted traction.

These primary sedimentary structures have been modified and obscured by subsequent bioturbation and by diagenetic processes (Fig. 16). The coarser-grained calcarenite layers became cemented during early diagenesis, preventing compaction. Therefore, the globigerinid tests are typically well-preserved within these well-lithified layers (Figs 12C and 15C), although high percentages of fragmented globigerinid tests may be admixed within some layers (Fig. 13D). The finer-grained interlayers were prone to chemical compaction by pressure dissolution and gave way to the formation of dissolution seams (Figs 13A and 14E). Within these fissile interlayers, globigerinid tests became collapsed, dissected and partly dissolved. As a result, the lithological contrast between the coarser-grained and finer-grained layers within the calcarenite beds has been strengthened during chemical compaction. It is unclear to which extent an unequal distribution of (unpreserved) pteropod shells has controlled the differentiation into cemented (non-compacted) and compacted layers. Pteropod shells are a typical constituent of Mediterranean pelagic oozes (Janssen & Peijnenburg, 2014) and consist of aragonite, which has a higher diagenetic potential compared to calcite (globigerinids and coccoliths) (Heath & Mullins, 1984). Together with increasing porosity, aragonite is a catalyst to initiate early diagenetic cementation (Bathurst, 1975; Eberli & Betzler, 2019).

The controlling mechanism behind the short-term fluctuating flow strength is unknown, as is the actual duration of 'short-term'. Various short-term oscillating energy conditions have been described from thermohaline and wind-driven bottom currents (see Shanmugam, 2008). An entire thick calcarenite bed (C3 division) is thought to have been deposited from a vigorous bottom current whose flow strength fluctuated irregularly (or even rhythmically). The authors suggest that fluctuating bottom currents are the norm during the deposition of all contourite divisions, including the accumulation of the calcilutite beds (C1 divisions). The properties of such fine-grained sediment calcilutites, however, do not clearly record the varying flow strength, although some of the calcilutite beds studied also show a faint wavy layering. Nevertheless, the standard bi-gradational sequence model (Gonthier *et al.*, 1984; Stow & Faugères, 2008) clearly shows an irregular silt–mud alternation in the C2 and C4 divisions, which these authors interpreted as due to short-term fluctuation in dynamic properties of the bottom current.

Turbidites versus contourites: diagnostic criteria based on microfacies

One of the principal differences between calcareous turbidites and contourites in this study results from different sediment provenances for the gravity-flow and bottom-current controlled processes, respectively. Turbidites are dominated by benthic thick-shelled bioclasts supplied from euphotic shallow-marine settings, whereas contourites comprise mainly skeletons of planktonic biota recycled from deep-marine pelagic muds. Three cases with respect to particle composition (due to different provenance) must be considered:

1 Where exclusively skeletons of planktonic organisms occur (typically fine-grained deposits, calcarenites and calcilutites), the distinction between turbidites and contourites can best be made based on depositional texture. **Turbidite** beds show a clear trend from particle-supported textures (globigerinid grainstone) to mud-supported textures (globigerinid wackestone). The lower part of the typically sharp-based turbidite beds preserves well-defined lamination (parallel and cross-lamination) that contrasts with the intensively bioturbated tops (with increasing homogenization towards the top). **Contourite** beds show more irregular and stepwise trends from mud-supported (globigerinid wackestone) to grain-supported (globigerinid packstone) and back again to mud-supported (globigerinid wackestone) depositional textures. Contourite beds typically show indistinct lower and upper boundaries and similar intensity of bioturbation in the lower and upper parts of the bed. The particle-supported middle part of a contourite bed is typically more mud rich (globigerinid packstone) and heterogeneous compared to the particle-supported lower part of a turbidite bed (globigerinid grainstone). These differences result from the fact that turbidites are produced by short-lived depositional events that are followed by bioturbation, whereas contourites arise from a continuous accumulation process that is accompanied by bioturbation throughout.

2 Where skeletons of planktonic organisms prevail but subordinate amounts of shallow-water bioclasts occur (typically medium-grained deposits, calcarenites), the distinction between turbidites and contourites can best be made based on particle distribution related to sedimentary structures. **Turbidite** beds show a clear trend from particle-supported textures (grainstone and packstone) to mud-supported textures (wackestone). The lower part of the typically sharp-based and normally-graded turbidite beds commonly includes intraclasts and comprises a distinctly higher proportion of shallow-water bioclasts (decreasing upward). **Contourite** beds, which show a well-developed wavy layering with local faint lamination or rarely-preserved parallel and cross-lamination (within non-compacted layers), are characterized by a layer-specific amount of shallow-water bioclasts. The proportion of those robust bioclasts may decrease or increase from layer to layer; individual layers may even be free of shallow-water bioclasts. Sorting within these particle-supported layers (packstone and grainstone) is generally low. These differences result from the fact that turbidite beds are produced by a single event whereas the wavy-bounded layers of the contourites (C3 divisions) represent more permanent deposition under fluctuating current conditions, resulting in intermittent sediment accretion.

3 Where skeletons of shallow-water organisms prevail (typically coarse-grained deposits, calcarenites and calcirudites), the deposit is typically a turbidite or a bottom-current reworked turbidite top. The generally sharp-based **turbidite** beds are structureless (deposits of concentrated density flows) or show (parts of) the classical Bouma sequence (deposits of turbulent density flows). They are better sorted than contourites of similar grain size. Robust bioclastic material from euphotic shallow-water sources (mainly benthos) constitute a distinct particle-supported depositional fabric. Intraclasts and a subordinate amount of planktonic bioclasts are embedded, both of which have been incorporated by seabed erosion due to the erosive capacity of the density flow. The **bottom-current reworked turbidite top** displays both a centimetre-scale layering (with crude lamination) and repeated inverse to normal grading within these layers. These transitional sediments, between turbidites and contourites, are less well-sorted and the amount of shallow-water bioclasts deceases layer by layer.

The marked differences in the nature of transport and deposition by turbidity currents and bottom currents have fundamental consequences for the nature of the respective deposits and the preservation of both primary sedimentary structures and secondary bioturbational structures.

Turbidites are typically produced by short-lived, rapid depositional events that temporarily interrupt the normal activity of bottom-dwelling organisms (Bouma, 1962; Stow & Shanmugam, 1980; Mulder, 2011). Sediment deposition is controlled by rapidly decreasing flow strength, which typically results in normal grading and a distinct sequence of primary sedimentary structures (for example, the Bouma sequence, partial Bouma sequence or modified Bouma sequence in carbonates). Bioturbation is resumed post-deposition and therefore works downward from the upper boundary of the turbidite bed, which leaves primary sedimentary structures within the lower part of a turbidite bed generally undisturbed (Uchman & Wetzel, 2011; Rodríguez-Tovar & Hernández-Molina, 2018).

Contourites, by contrast, result from relatively weak and semi-continuous sediment deposition and intermittent reworking that is mostly accompanied by continuous bioturbation (McCave, 2008; Stow *et al.*, 2008). Sediment accumulation may repeatedly change between bed-load-dominated and suspension-load-dominated deposition, and include periods of erosion and sediment winnowing. Bioturbation is penecontemporaneous with sedimentation, even intermittent during accumulation of the coarse-grained contourites. Its intensity varies mainly due to changing hydrodynamic conditions and food supply, favouring or suppressing burrowing benthic communities (Wetzel *et al.*, 2008). Consequently, primary sedimentary structures (traction structures, inverse and normal grading) are generally less well-preserved in contourites (especially in fined-grained contourites), as well as reflecting changing conditions of short-term higher accumulation rates, lower bioturbation rates and flow instability.

Pelagites versus muddy contourites: diagnostic criteria based on microfacies

The distinction of pelagic oozes from muddy calcareous contourites is difficult, since all of these fine-grained sediments form relatively uniform records showing indistinct bedding based on subtle compositional variation. In pelagic environments, this longer-duration compositional variation typically results from biogenic productivity fluctuations and alternating seafloor redox conditions (e.g. Berger, 1988; Tateo *et al.*, 2000; Falkowski, 2002; Damholt & Surlyk, 2004; Hüneke & Henrich, 2011). In bottom-current controlled environments, both sediment supply and deposition are varying (e.g. Llave *et al.*, 2006; Hüneke & Stow, 2008; Stow *et al.*, 2008; Faugères & Mulder, 2011, 2011; Rebesco *et al.*, 2014). The fluctuating flow strength includes changing additional food supply that causes temporary high faunal abundance and enhanced rates of burrowing (Wetzel *et al.*, 2008). Consequently, within all of these environments, a diverse set of controls may give way to a very indistinctly-defined bedding, which is modified by bioturbational sequences.

The key point is that sediment re-location and mixing from different sources occurs only in bottom-current controlled environments. Within intra-particle pores of some of the skeletal grains (for example, globigerinids) of the muddy calcareous contourites, sediment that is different from the surrounding matrix can be identified (Fig. 17). The material trapped within these shells preserves the mud composition of the source area. Thus, such allochthonous bioclasts are indicative of erosional reworking and re-deposition. Within pelagic sediments, by contrast, shells are empty or filled with mud that is identical to the overall matrix.

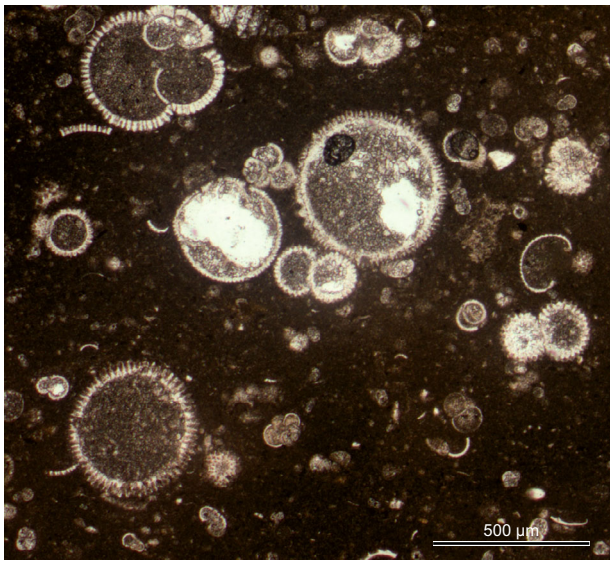

Fig. 17. Microfacies of calcilutites (F2a, globigerinid wackestone), which are interbedded with calcarenites (F3c, globigerinid packstone–grainstone). See Fig. 3 for general lithology. Middle Miocene from the Pakhna Formation (Sample Pet 34). Interpretation: muddy calcareous contourites. Note the differing characteristics (grain size and colour) of the matrix within and around the globigerinid test, which is indicative of reworking and redeposition.

CONCLUSIONS

The contourite drift formed during the Eocene to middle Miocene at the palaeoslope south of Cyprus consists of muddy and sandy calcareous bottom-current deposits (calcilutites and calcarenites) that are interbedded with pelagic carbonates (calcilutites and rare chert intercalations) and hemipelagic deposits (marls). In addition, calcareous turbidites (calcarenites and calcirudites) and other types of gravity-driven density-flow deposits are interstratified. Thin distal (fine-grained) turbidites occur in the Eocene, while thicker proximal (coarse-grained) turbidites are identified in the Miocene part of

the studied record. These turbidites reveal a distal lower slope (Eocene) to middle slope (early and middle Miocene) setting of the contourite depositional system.

Calcareous contourites can be identified and differentiated from turbidites by means of microfacies characteristics, since bottom currents flow parallel to regional slope, while gravity flows are downslope processes, which has implications for sediment provenance and particle composition. Carbonate microfacies, however, is indicative for contourites and turbidites only in combination with compositional characteristics and bed-scale features such as grading (inverse to normal / normal), bed-boundary characteristics (gradual base / sharp base), preservation of primary traction structures (rarely preserved in lower and upper part / well-preserved in lower parts only). What is essential is the relative ratio of planktonic to shallow-water particles and its bed-related spatial distribution (layer-specific amount / bioturbationally mottled / grading-related distribution).

Muddy calcareous bottom-current deposits constitute, together with pelagic carbonates, most of the Eocene record. Both are represented by calcilutites consisting of heavily bioturbated globigerinid wackestone, making a clear-cut distinction difficult.

Sandy calcareous bottom-current deposits prevail during the Miocene and are represented by: (i) thin calcarenite beds (<5 cm); and (ii) thick calcarenite beds with internal wavy layering (5 to 60 cm). Both types of calcarenites usually show gradual bed boundaries, which display under the microscope a transition from mud to particle-support and vice versa. Some of the thick calcarenite beds are more distinctly bounded, even sharply bounded, at least macroscopically, due to the carbonate-specific sediment properties (bimodal grain-size distribution and different specific weight of the particles) as detailed by Eberli & Betzler (2019). However, bed boundaries are not erosional. Both types of calcarenite beds form bi-gradational cycles of grain-size and depositional texture together with underlying and overlying calcilutite beds. This bed-scale cyclicity is interpreted to be caused by long-term fluctuations of the flow strength, as is typical of a bottom-current controlled deep-marine environments.

The thick wavy-layered calcarenite beds, which also include lenticular, flaser and parallel layering, locally preserve relic lamina sets of parallel and cross-lamination within individual (non-compacted) calcarenite layers. The wavy layering is interpreted to result from a repeated change between bedload deposition and suspension fallout caused by short-term fluctuations of the bottom-current flow strength (of hitherto unknown origin). Thus, the vertical stacked contourite sequences reflect a cyclicity of the forcing variables at two different timescales.

Microfacies characteristics and bed-scale sedimentary structures indicate that there has been interaction between contour currents and gravity flows. Both partial reworking of turbidite tops and complete obliteration of turbidite beds occurred. In both cases, the reworking of shallow-water-derived bioclasts gave way to recycling and embedding of those coarse-grained particles within sandy contourites.

Based on this key study, future work requires a description of the large-scale spatial facies variability and lateral thickness variations together with the identification of erosive features along the Cyprus palaeo-margin, which should be related to the large-scale architecture and orientation of the contourite depositional system. Proximal–distal trends of sediment composition and depositional textures must be revealed for reconstructing the palaeoceanographic setting and the transport pathways of both bottom-current induced along-slope redistribution and gravity-driven down-slope supply. This approach should integrate drift-scale features, bed-scale sedimentary characteristics, microfacies and ichnological data.

ACKNOWLEDGEMENTS

The authors acknowledge the scientific discussions and input from Adriano Viana and other colleagues who participated during our field campaigns in 2017 and 2018. The research was partially supported through the Spanish Ciencia y Tecnologías Marinas projects CTM 2012-39599-C03, CGL2016-80445-R (AEI/FEDER, UE) and CTM2016-75129-C3-1-R, and conducted in the framework of "The Drifters Research Group" of the Royal Holloway University of London (RHUL). Research by RT was funded by Projects CGL2015-66835-P, PID2019-104625RB-100P (Secretaría de Estado de I+D+I, Spain), B-RNM-072-UGR18 (FEDER Andalucía), and P18-RT-4074 (Junta de Andalucía), and Scientific Excellence Unit UCE-2016-05 (Universidad de Granada). Sylvia Weinert is thanked for the production of many excellent thin sections. Constructive and careful reviews by

Thierry Mulder and two anonymous reviewers helped to reorganize and to sharpen the concept presented in this contribution. In addition, we thank the Associate Editors Catherine Reid, Jody Webster and the Editor of *Sedimentology* Giovanna Della Porta for their perceptive comments, which contributed significantly in improving the paper. Open access funding enabled and organized by Projekt DEAL (University of Greifswald in the Alliance of German Science Organizations).

CONFLICT OF INTEREST

We declare that we do not have any commercial or associative interest that represents a conflict of interest in connection with the work submitted.

DATA AVAILABILITY STATEMENT

The data that support the findings of this study are available from the corresponding author upon reasonable request.

REFERENCES

Baccelle, L. and **Bosellini, A.** (1965) Diagrammi per la stima visiva della composizione percentuale nelle rocce sedimentarie. *Ann. Univ. Ferrara N.S. Sez. IX. Sci. Geol. Paleont.*, **1**, 59–62.

Bathurst, R.G.C. (1975) *Carbonate Sediments and Their Diagenesis*. Elsevier, Amsterdam, 657 pp.

Berger, A. (1988) Milankovitch theory and climate. *Rev. Geophys.*, **26**, 624–657.

Berger, W.H. and **Piper, D.J.W.** (1972) Planktonic foraminifera: differential settling, dissolution, and redeposition. *Limnol. Oceanogr.*, **17**, 275–287.

Beavington-Penney, S.J. and **Racey, A.** (2004) Ecology of extant nummulitids and other larger benthic foraminifera: applications in palaeoenvironmental analysis. *Earth-Sci. Rev.*, **67**, 219–265.

Bouma, A.H. (1962) *Sedimentology of Some Flysch Deposits. A Graphic Approach to Facies Interpretation*. Elsevier, Amsterdam, 168 pp.

Brackenridge, R.E., **Stow, D.A.V.**, **Hernández-Molina, F.J.**, **Mena, A.**, **Llave, E.**, **Jones, C.**, **Alejo, I.**, **Ercilla, G.**, **Frances, G.**, **Nombela, M.A.**, **Perez-Arlucea, M.** and **Ducassou, E.** (2018) Textural characteristics and facies of sand-rich contourite depositional systems. *Sedimentology*, **65**, 2223–2252.

Bush, A.B. (1997) Numerical simulation of the Cretaceous Tethys circum-global current. *Science*, **275**, 807–810.

Butzin, M., **Lohmann, G.** and **Bickert, T.** (2011) Miocene ocean circulation inferred from marine carbon cycle modeling combined with benthic isotope records. *Paleoceanography*, **26**, PA1203.

Capella, W., **Hernández-Molina, F.J.**, **Flecker, R.**, **Hilgen, F.J.**, **Hssain, M.**, **Kouwenhoven, T.J.**, **van Oorschot, M.**, **Sierro, F.J.**, **Stow, D.A.V.**, **Trabucho-Alexandre, J.**, **Tulbure, M.A.**, **de Weger, W.**, **Yousfi, M.Z.** and **Krijgsman, W.** (2017) Sandy contourite drift in the late Miocene Rifian Corridor (Morocco): Reconstruction of depositional environments in a foreland-basin seaway. *Sed. Geol.*, **355**, 31–57.

Chaisson, W.P. and **Leckie, R.M.** (1993) High-resolution Neogene planktonic foraminifer biostratigraphy of Site 806, Ontong Java Plateau (western equatorial Pacific). *Proc. ODP, Sci. Results*, 130, College Station, TX, Ocean Drilling Program Management International Inc.

Chiarella, D., **Longhitano, S.G.** and **Tropeano, M.** (2017) Types of mixing and heterogeneities in siliciclastic-carbonate sediments. *Mar. Petrol. Geol.*, **88**, 617–627.

Constantinou, G. (1995) *Geological Map of Cyprus, Scale 1/250.000*. Geological Survey of Cyprus, Nicosia, 1 pp.

Damholt, T. and **Surlyk, F.** (2004) Laminated–bioturbated cycles in Maastrichtian chalk of the North Sea: oxygenation fluctuations within the Milankovitch frequency band. *Sedimentology*, **51**, 1323–1342.

Decalf, C., **Stirling, E.J.** and **Hossack, J.** (2016) Contourite deposition over time along the offshore Tanzania Margin: Controls, Architectures, and effects on Hydrocrabon propectivity. In: *East Africa: from Research to Reserves*. Conference, The Geological Society, 13–15 April, Abstract volume.

de Castro, S., **Hernández-Molina, F.J.**, **Rodríguez-Tovar, F.J.**, **Llave, E.**, **Ng, Z.L.**, **Nishida, N.** and **Mena, A.** (2020) Contourites and bottom current reworked sands: bed facies model and implications. *Mar. Geol.*, **428**, 106267.

de la Vara, A. and **Meijer, P.** (2016) Response of Mediterranean circulation to Miocene shoaling and closure of the Indian Gateway: a model study. *Palaeogeogr. Palaeoclimatol. Palaeoecol.*, **442**, 96–109.

Dunham, R.J. (1962) Classification of carbonate rocks according to depositional texture. In: *Classification of Carbonate Rocks* (Ed. Ham, W.E.), *AAPG Mem.*, **1**, 108–121.

Eaton, S. and **Robertson, A.** (1993) The Miocene Pakhna Formation, southern Cyprus and its relationship to the Neogene tectonic evolution of the Eastern Mediterranean. *Sed. Geol.*, **86**, 273–296.

Eberli, G.P. (1991) Calcareous turbidites and their relationship to sea-level fluctuations and tectonism. In: *Cycles and Events in Stratigraphy* (Eds Einsele, G., Ricken, W. and Seilacher, A.), pp. 340–359. Springer, Berlin.

Eberli, G.P. and **Betzler, C.** (2019) Characteristics of modern carbonate contourite drifts. *Sedimentology*, **66**, 1163–1191.

Edwards, S., **Hudson-Edwards, K.**, **Cann, J.**, **Malpas, J.** and **Xenophontos, C.** (2010) *Cyprus. Classic Geology in Europe 7*. Terra Publishing, Dunedin Academic Press Ltd., Harpenden, 271 pp.

Embry, A.F. and **Klovan, J.E.** (1972) Absolute water depth limits of Late Devonian palecological zones. *Geol. Rundsch.*, **61**, 672–686.

Falkowski, P.G. (2002) The ocean's invisible forest—marine phytoplankton play a critical role in regulating the earth's climate. Could they also be used to combat global warming? *Sci. Am.*, **287**, 54–61.

Famakinwa, S.B., **Shanmugam, G.** and **Nieto, J.** (1997) Bottom-current reworked sands – a 'new' latent reservoir type in deep-water sedimentation, Equatorial Guinea and Nigeria. *AAPG Bull.*, **81**, 34–44.

Faugères, J.-C. and **Mulder, T.** (2011) Contour currents and contourite drifts. In: *Deep-Sea Sediments* (Eds Hüneke, H. and Mulder, T.), *Dev. Sedimentol.*, **63**, 149–214.

Ferguson, R., **Kane, I.**, **Fuhrmann, A.**, **Barker, S.**, **Siversen, C.**, **Brunt, R.** and **Martinsen, O.J.** (2018) Progressive Confinement and Downslope Propagation of Submarine Slope Channels. AAPG, ACE2018, 20–23 May, Salt Lake City, Utah.

Flügel, E. (2010) *Microfacies of Carbonate Rocks. Analysis, Interpretation and Application*. Springer, Berlin, 976 pp.

Folk, R.L. (1959) Practical petrographic classification of limestones. *AAPG Bull.*, **43**, 1–38.

Folk, R.L. (1962) Spectral subdivision of limestone types. In: *Classification of Carbonate Rocks* (Ed. Ham, W.E.), *AAPG Mem.*, **1**, 62–84.

Folk, R.L. and **Ward, W.C.** (1957) A study in the significance of grain-size parameters. *J. Sed. Petrol.*, **27**, 3–26.

Follows, E.J. (1992) Patterns of reef sedimentation and diagenesis in the Miocene of Cyprus. *Sed. Geol.*, **79**, 225–253.

Fonnesu, M., **Palermo, D.**, **Galbiati, M.**, **Marchesini, M.**, **Bonamini, E.** and **Bendias, D.** (2020) A new world-class deep-water play-type deposited by the syndepositional interaction of turbidity flows and bottom currents: The giant Eocene Coral Field in northern Mozambique. *Mar. Petrol. Geol.*, **111**, 179–201.

Frenz, M., **Baumann, K.-H.**, **Boeckel, B.**, **Hoppner, R.** and **Henrich, R.** (2005) Quantification of foraminifer and coccolith carbonate in South Atlantic surface sediments by means of carbonate grain-size distributions. *J. Sed. Res.*, **75**, 464–475.

Fuhrmann, A., **Kane, I.**, **Ferguson, R.**, **Barker, S.**, **Siversen, C.** and **Brunt, R.** (2018) Drift Influence on Deep-Marine Slope Channel Facies and Geometries: Implications for Reservoir Quality Distribution – Block 2, Offshore Tanzania. AAPG, ACE2018, 20–23 May, Salt Lake City, Utah.

Gong, C., **Wang, Y.**, **Zheng, R.**, **Hernández-Molina, J.**, **Li, Y.**, **Stow, D.**, **Xu, Q.** and **Brackenridge, R.E.** (2016) Middle Miocene reworked turbidites in the Baiyun Sag of the Pearl River Mouth Basin, northern South China Sea margin: Processes, genesis, and implications. *J. Asian Earth Sci.*, **128**, 116–129.

Gonthier, E., **Faugères, J.-C.** and **Stow, D.A.V.** (1984) Contourite facies of the Faro Drift, Gulf of Cadiz. In: *Fine-Grained Sediments, Deep-Water Processes and Facies* (Eds Stow, D.A.V. and Piper, D.J.W.), *Geol. Soc. London Spec. Publ.*, **15**, 275–292.

Grabau, A.W. (1904) On the classification of sedimentary rocks. *Amer. Geol.*, **33**, 228–247.

Hallam, A. (1969) Faunal realms and facies in the Jurassic. *Paleontology*, **12**, 1–18.

Harzhauser, M., **Kroh, A.**, **Mandic, O.**, **Piller, W.E.**, **Göhlich, U.**, **Reuter, M.** and **Berning, B.** (2007) Biogeographic responses to geodynamics: a key study all around the Oligo-Miocene Tethyan Seaway. *Zool. Anz.*, **246**, 241–256.

He, Y., **Duan, T.** and **Gao, Z.** (2008) Sediment entrainment. In: *Contourites* (Eds Rebesco, M. and Camerlenghi, A.), *Dev. Sedimentol.*, **60**, 101–120.

Heath, K.C. and **Mullins, H.T.** (1984) Open-ocean, off-bank transport of fine-grained carbonate sediment in the Northern Bahamas. *Geol. Soc.*, **15**, 199–208.

Henrich, R. and **Hüneke, H.** (2011) Hemipelagic advection and periplatform sedimentation. In: *Deep-Sea Sediments* (Eds Hüneke, H. and Mulder, T.), *Dev. Sedimentol.*, **63**, 353–396.

Hernández-Molina, F.J., **Hüneke, H.**, **Rodriguez-Tovar, F.J.**, **Llave, E.**, **Ng, Z.L.**, **Chiarella, D.**, **Suklap, S.**, **Docherty, B.**, **Mena, A.** and **Stow, D.A.W.**(2018) Deep-water bottom current deposits from Cyprus: an ancient analogue for contourite terraces and plastered drifts? 20th Int. Sedimentological Congress, 13-17 August 2018. Quebec, Canada. Abstracts.

Herold, N., **Huber, M.**, **Müller, R.D.** and **Seton, M.** (2012) Modeling the Miocene climatic optimum: ocean circulation. *Paleoceanography*, **27**, PA1209.

Hesemann, M. (2015) The foraminifera.eu database: concept and status. *Palaeontol. Electron.*, **18.3.48A**, 1–14.

Hesemann, M. (2018) Foraminifera.eu Project Database. Accessed at: http://www.foraminifera.eu/single.php?no=1009861&aktion=suche.

Hicks, S.B. (2014) Paleoecology and sedimentology of the volcanically active Late Eocene continental shelf, Northeast Otago, New Zealand. Unpublished PhD thesis, University of Otago, Otago, 245 pp.

Huang, Y.T., **Yao, G.Q.**, **Zhou, F.D.** and **Wang, T.T.** (2017) Impact factors on reservoir quality of elastic Huangliu formation in overpressure diapir zone, Yinggehai Basin, China. *J. Petrol. Sci. Eng.*, **154**, 322–336.

Hüneke, H. (2007) Pelagic carbonate ooze reworked by bottom currents during Devonian approach of the continents Gondwana and Laurussia. In: *Economic and Palaeoceanographic Significance of Contourite Deposits* (Eds Viana, A.R. and Rebesco, M.), *Geol. Soc. London Spec. Publ.*, **276**, 299–328.

Hüneke, H. (2013) Bioclastic contourites: depositional model for bottom-current redeposited pelagic carbonate ooze (Devonian, Moroccan Central Massif). *Z. Dt. Ges. Geowiss. (German J. Geosci.)*, **164**, 253–277.

Hüneke, H. and **Henrich, R.** (2011) Pelagic sedimentation in modern and ancient oceans. In: *Deep-Sea Sediments* (Eds Hüneke, H. and Mulder, T.), *Dev. Sedimentol.*, **63**, 215–351.

Hüneke, H. and **Stow, D.A.V.** (2008) Identification of ancient contourites: problems and palaeoceanographic significance. In: *Contourites* (Eds Rebesco, M. and Camerlenghi, A.), *Dev. Sedimentol.*, **60**, 323–344.

Iaccarino, S. and **Premoli Silva, I.** (1979) Paleogene planktonic foraminiferal biostratigraphy of DSDP Hole 398D, Leg 47B, Vigo Seamount, Spain. Init. Repts. DSDP, 47, Part 2 of the cruises of the drilling vessel Glomar Challenger, Vigo, Spain to Brest, France, April-May 1976. Deep-Sea Drilling Program Management International Inc.

Ito, M. (2002) Kuroshio current-influenced sandy contourites from the Plio-Pleistocene Kazusa forearc basin, Boso Peninsula, Japan. In: *Deep-Water Contourite Systems: Modern Drifts and Ancient Series, Seismic and Sedimentary Characteristics* (Eds Stow, D.A.V., Pudsey, C.J., Howe, J.A., Faugères, J.-C. and Viana, A.R.), *Geol. Soc. Mem.*, **22**, 421–432.

Janssen, A.W. and **Peijnenburg, K.T.C.A.** (2014) Holoplanktonic Mollusca: Development in the Mediterranean Basin during the last 30 million years and their future. In: *The Mediterranean Sea* (Eds Goffredo, S. and Dubinsky, Z.), pp. 341–362. Springer, Amsterdam.

Jovane, L., **Coccioni, R.**, **Marsili, A.** and **Acton, G.** (2009) The late Eocene greenhouse-icehouse transition: Observations from the Massignano global stratotype section and point (GSSP). In: *The Late Eocene Earth – Hothouse, Icehouse, and Impacts* (Eds Koeberl, C. and Montanari, A.), *Geol. Soc. Am. Spec. Pap.*, **452**, 149–168.

Kahler, G. (1994) Stratigraphy and sedimentology of the Paleogene Lefkara Formation, Cyprus. Unpublished PhD thesis, University of Southampton, Southampton, 319 pp.

Kahler, G. and **Stow, D.A.V.** (1998) Turbidites and contourites of the Palaeogene Lefkara Formation, southern Cyprus. *Sed. Geol.*, **115**, 215–231.

Kay, G.M. (1951) North American geosynclines. *Geol. Soc. Am. Mem.*, **48**, 1–143.

Krapp, M. and **Jungclaus, J.H.** (2011) The Middle Miocene climate as modelled in an atmosphere–ocean biosphere model. *Clim. Past*, **7**, 1169–1188.

Lee, I. and **Ogawa, Y.** (1998) Bottom-current deposits in the Miocene-Pliocene Misaki Formation, Izu forearc area, Japan. *Island Arc*, **7**, 315–329.

Llave, E., **Schönfeld, J.**, **Hernández-Molina, F.J.**, **Mulder, T.**, **Somoza, L.**, **Diaz del Rio, V.D.** and **Sanchez-Almazo, I.** (2006) High-resolution stratigraphy of the Mediterranean outflow contourite system in the Gulf of Cadiz during the Late Pleistocene. The impact of Heinrich events. *Mar. Geol.*, **227**, 241–262.

Longiaru, S. (1987) Visual comparators for estimating the degree of sorting from plane and thin section. *J. Sed. Petrol.*, **57**, 791–794.

Lord, A.R., **Harrison, R.W.**, **BouDagher-Fadel, M.**, **Stone, B.D.** and **Varol, O.** (2009) Miocene mass-transport sediments, Troodos Massif. *Cyprus. Proc. Geol. Assoc.*, **120**, 133–138.

Lovell, J.P.B. and **Stow, D.A.V.** (1981) Identification of ancient sandy contourites. *Geology*, **9**, 347–349.

Mantis, M. (1970) Upper Cretaceous – Tertiary foraminiferal zones in Cyprus. *Sci. Res. Cent. Cyprus. Epetiris*, **3**, 227–241.

Martín-Chivelet, J., **Fregenal-Martínez, M.A.** and **Chacón, B.** (2008) Traction structures in contourites. In: *Contourites* (Eds Rebesco, M. and Camerlenghi, A.), *Dev. Sedimentol.*, **60**, 159–182.

Matthew, A.J., **Woods, A.J.** and **Oliver, C.** (1991) Spots before eyes: new comparison charts for visual percentage estimation in archaeological material. In: *Recent Developments in Ceramic Petrology* (Eds Middleton, A. and Freestone, I.), *Brit. Mus. Occasional Paper*, **81**, 211–263.

McCave, I.N. (2008) Size sorting during transport and deposition of fine sediments: sortable silt and flow speed. In: *Contourites* (Eds Rebesco, M. and Camerlenghi, A.), *Dev. Sedimentol.*, **60**, 121–142.

McCave, I.N. and **Hall, I.R.** (2006) Size sorting in marine muds: processes, pitfalls and prospects for palaeoflow-speed proxies. *Geochem. Geophys. Geosyst.*, **7**, Q10N05.

Meulenkamp, J.E. and **Sissingh, W.** (2003) Tertiary palaeogeography and tectonostratigraphic evolution of the Northern and Southern Peri-Tethys platforms and the intermediate domains of the African-Eurasian convergent plate boundary zone. *Palaeogeogr. Palaeoclimatol. Palaeoecol.*, **196**, 209–228.

Miguez-Salas, O. and **Rodríguez-Tovar, F.J.** (2019a) Stable deep-sea macrobenthic trace maker associations in disturbed environments from the Eocene Lefkara Formation, Cyprus. *Geobios*, **52**, 37–45.

Miguez-Salas, O. and **Rodríguez-Tovar, F.J.** (2019b) Ichnofacies distribution in the Eocene-Early Miocene Petra Tou Romiou outcrop, Cyprus: sea level dynamics and palaeoenvironmental implications in a contourite environment. *Int J Earth Sci*, **108**, 2531–2544.

Miguez-Salas, O., **Rodríguez-Tovar, F.J.** and **Uchman, A.** (2019a) A new teichichnoid trace fossil *Syringomorpha cyprensis* from the Miocene of Cyprus. *Palaios*, **34**, 506–514.

Miguez-Salas, O., **Dorador, J.** and **Rodríguez-Tovar, F.J.** (2019b) Introducing Fiji and ICY image processing techniques in ichnological research as a tool for sedimentary basin analysis. *Mar Geol*, **413**, 1–9.

Miller, M.C. and **Komar, P.D.** (1977) Development of sediment threshold curves for unusual environments (Mars) and for inadequately studied materials (foram sands). *Sedimentology*, **24**, 709–721.

Moores, E.M. and **Vine, F.J.** (1971) The Troodos massif, Cyprus and other ophiolites as oceanic crust: evaluation and implications. *Philos. Trans. R. Soc. London A*, **268**, 443–466.

Moraes, M.A.S., **Maciel, W.B.**, **Braga, M.S.S.** and **Viana, A.R.** (2007) Bottom-current reworked Palaeocene-Eocene deep-water reservoirs of the Campos Basin, Brazil. In: *Economic and Palaeoceanographic Significance of Contourite Deposits* (Eds Viana, A.R. and Rebesco, M.), *Geol. Soc. London Spec. Publ.*, **276**, 81–94.

Mulder, T. (2011) Gravity processes on continental slope, rise and abyssal plains. In: *Deep-Sea Sediments* (Eds Hüneke, H. and Mulder, T.), *Dev. Sedimentol.*, **63**, 25–148.

Mulder, T. and **Alexander, J.** (2001) The physical character of subaqueous sedimentary density currents and their deposits. *Sedimentology*, **48**, 269–299.

Mulder, T., **Ducassou, E.**, **Hanquiez, V.**, **Principaud, M.**, **Fauquembergue, K.**, **Tournadour, E.**, **Chabaud, L.**, **Reijmer, J.**, **Recouvreur, A.**, **Gillet, H.**, **Borgomano, J.**, **Schmitt, A.** and **Moal, P.** (2019) Contour current imprints and contourite drifts in the Bahamian archipelago. *Sedimentology*, **66**, 1192–1221.

Mulder, T., **Faugères, J.-C.** and **Gonthier, E.** (2008) Mixed turbidite-contourite systems. In: *Contourites* (Eds Rebesco, M. and Camerlenghi, A.), *Dev. Sedimentol.*, **60**, 435–456.

Mulder, T., **Hassan, R.**, **Ducassou, E.**, **Zaragosi, S.**, **Gonthier, E.**, **Hanquiez, V.**, **Marches, E.** and **Toucanne, S.** (2013) Contourites in the Gulf of Cadiz: a cautionary note on potentially ambiguous indicators of bottom current velocity. *Geo-Mar. Lett.*, **33**, 357–367.

Mullins, H.T., **Neumann, A.C.**, **Wilber, R.J.**, **Hine, A.C.** and **Chinburg, S.J.** (1980) Carbonate sediment drifts in northern Straits of Florida. *AAPG Bull.*, **64**, 1701–1717.

Omta, A.W. and **Dijkstra, H.A.** (2003) A physical mechanism for the Atlantic-Pacific flow reversal in the early Miocene. *Global Planet. Change*, **36**, 265–276.

Palamakumbura, R.N. and **Robertson, A.H.F.** (2018) Pliocene-Pleistocene sedimentary–tectonic development of the Mesaoria (Mesarya) Basin in an incipient, diachronous collisional setting: facies evidence from the north of Cyprus. *Geol. Mag.*, **155**, 997–1022.

Palermo, D., **Galbiati, M.**, **Famiglietti, M.**, **Marchesini, M.**, **Mezzapesa, D.** and **Fonnesu, F.** (2014) Insights into a New Super-Giant Gas Field – sedimentology and Reservoir Modelling of the Coral Complex, Offshore Northern Mozambique. Offshore Technology Conference Asia, Kuala Lumpur, Malasya, 25–28 March, 2014, OTC-24907-MS, 1–8.

Pantazis, T.M. (1967) The Geology and mineral resources of the Pharmakas – Kalavasos Area. *Cyprus Geol. Surv. Dept. Mem.*, **9**, 1–120.

Papadimitriou, N., **Deschamps, R.**, **Symeou, V.**, **Souque, C.**, **Gorini, C.**, **Nader, F.H.** and **Blanpied, C.** (2018) The tectonostratigraphic evolution of Cenozoic basins of the Northern Tethys: the Northern margin of the Levant Basin. *Oil Gas Sci. Technol. Rev. IFP Ener. Nouvelles*, **73**, 1–27.

Pearson, P.N. and **Chaisson, W.P.** (1997) Late Paleocene to middle Miocene planktonic foraminifer biostratigraphy of

the Ceara Rise. In: Proc. ODP, Sci. Results, **154**, 33–68, College Station, TX, Ocean Drilling Program Management International Inc.

Peybernes, B., **Fondecave-Wallez, M.J.** and **Cugny, P.** (2005) Diachronism in the sedimentary cover around the Troodos ophiolitic massif (Cyprus). *Bull. Soc. Geol. France*, **176**, 161–169.

Rebesco, M., **Camerlenghi, A.** and **van Loon, A.J.** (2008) Contourite research: A field in full development. In: *Contourites* (Eds Rebesco, M. and Camerlenghi, A.), *Dev. Sedimentol.*, **60**, 1–10.

Rebesco, M., **Hernndez-Molina, F.J.**, **Van Rooij, D.** and **Wahlin, A.** (2014) Contourites and associated sediments controlled by deep-water circulation processes: state-of-the-art and future considerations. *Mar. Geol.*, **352**, 111–154.

Reolid, J. and **Betzler, C.** (2019) The ichnology of carbonate drifts. *Sedimentology*, **66**, 1427–1448.

Reuter, M., **Piller, W.E.**, **Harzhauser, M.**, **Mandic, O.**, **Berning, B.**, **Rögl, F.**, **Kroh, A.**, **Aubry, M.P.**, **Wielandt-Schuster, U.** and **Hamedani, A.** (2009) The Oligo-/Miocene Qom Formation (Iran): evidence for an early Burdigalian restriction of the Tethyan Seaway and closure of its Iranian gateways. *Int. J. Earth Sci.*, **98**, 627–650.

Robertson, A.H.F. (1976) Pelagic chalks and calciturbidites from the Lower Tertiary of the Troodos Massif, Cyprus. *J. Sed. Petrol.*, **46**, 1007–1016.

Robertson, A.H.F. (1977) Tertiary uplift history of the Troodos Massif, Cyprus. *Geol. Soc. Am. Bull.*, **88**, 1763–1772.

Robertson, A.H.F. (1990) Tectonic evolution of Cyprus. In: *Ophiolites: Oceanic Crustal Analogues* (Eds Malpas, J., Moores, E., Panayiotou, A. and Xenophontos, C.), *Proc Symposium 'Troodos 1987'. Cyprus Geol. Surv. Dept.*, **1990**, 235–250.

Robertson, A.H.F. and **Hudson, J.D.** (1974) Pelagic sediments in the Cretaceous and Tertiary history of the Troodos Massif, Cyprus. In: *Pelagic Sediments: on Land and under the Sea* (Eds Hsü, K.J. and Jenkyns, H.C.), *Int. Assoc. Sedimentol. Spec. Publ.*, **1**, 403–436.

Robertson, A.H.F. and **Woodcock, N.H.** (1979) Mamonia Complex, southwest Cyprus: evolution and emplacement of a Mesozoic continental margin. *Geol. Soc. Am. Bull.*, **90**, 651–665.

Rodríguez-Tovar, F.J. and **Hernández-Molina, F.J.** (2018) Ichnological analysis of contourites: past, present and future. *Earth-Sci. Rev.*, **182**, 28–41.

Rodríguez-Tovar, F.J., **Hernández-Molina, F.J.**, **Hüneke, H.**, **Chiarella, D.**, **Llave, E.**, **Mena, A.**, **Miguez-Salas, O.**, **Dorador, J.**, **de Castro, S.** and **Stow, D.A.V.** (2019a) Key evidence for distal turbiditic- and bottom-current interactions from tubular turbidite infills. *Palaeogeogr. Palaeoclimatol. Palaeoecol.*, **533**, 109233.

Rodríguez-Tovar, F.J., **Hernández-Molina, F.J.**, **Hüneke, H.**, **Llave, E.** and **Stow, D.A.V.** (2019b) Contourite facies model: Improving characterization of contourites based on the ichnological analysis. *Sed. Geol.*, **384**, 60–69.

Rögl, F. (1999) Mediterranean and Paratethys. Facts and hypotheses of an Oligocene to Miocene paleogeography (short overview). *Geol. Carpath.*, **50**, 339–349.

Sanfilippo, A., **Hakyemez, A.** and **Tekin, U.K.** (2003) Biostratigraphy of Late Paleocene – Middle Eocene radiolarians and foraminifera from Cyprus. *Micropaleontology*, **49**, 47–64.

Sansom, P. (2017) Turbidites versus Contourites: hybrid systems of the Tanzanian margin. Extended Abstract. In: 16th PESGB/HGS African E&P Conference, London, 31 Aug – 1 Sept 2017, Extended Abstract.

Shanmugam, G. (2008) Deep-water bottom currents and their deposits. In: *Contourites* (Eds Rebesco, M. and Camerlenghi, A.), *Dev. Sedimentol.*, **60**, 59–81.

Shanmugam, G. (2012) New perspectives on deep-water sandstones: origin, recognition, initiation, and reservoir quality. *Handbook of Petroleum Exploration and Production*, **9**. Elsevier, Amsterdam, 524 pp. Available at: https://www.elsevier.com/books/new-perspectives-on-deep-water-sandstones/shanmugam/978-0-444-56335-4

Shanmugam, G. (2017) Contourites: Physical oceanography, process sedimentology, and petroleum geology. *Petrol. Explor. Develop.*, **44**, 183–216.

Shanmugam, G. (2018) Comment on "Ichnological analysis of contourites: Past, present and future" by Francisco J. Rodríguez-Tovar and F. Javier Hernández-Molina [Earth-Sci. Rev., 182, 28–41]. *Earth-Sci. Rev.*, **184**, 46–49.

Shanmugam, G., **Spalding, T.D.** and **Rofheart, D.H.** (1993) Process sedimentology and reservoir quality of deep-marine bottom-current reworked sands (sandy contourites): an example from the Gulf of Mexico. *AAPG Bull.*, **77**, 1241–1259.

Sierro, F.J., **Flores, J.A.** and **Baraza, J.** (1999) Late glacial to recent paleoenvironmental changes in the Gulf of Cadiz and formation of sandy contourite layers. *Mar. Geol.*, **155**, 57–172.

Stanley, S.M. (1995) New horizons for paleontology, with two examples: the rise and fall of the Cretaceous Supertethys and the cause of the modern ice age. *J. Paleontol.*, **69**, 999–1007.

Stow, D.A.V. (1979) Distinguishing between fine-grained turbidites and contourites on the Nova Scotian deep-water margin. *Sedimentology*, **26**, 371–387.

Stow, D.A.V. and **Faugères, J.-C.** (2008) Contourite facies and the facies model. In: *Contourites* (Eds Rebesco, M. and Camerlenghi, A.), *Dev. Sedimentol.*, **60**, 223–250.

Stow, D.A.V. and **Shanmugam, G.** (1980) Sequence of structures in fine-grained turbidites: comparison of recent deep-sea and ancient flysch sediments. *Sed. Geol.*, **25**, 23–42.

Stow, D.A.V., **Braakenburg, N.E.** and **Xenophontos, C.** (1995) The Pissouri Basin fan-delta complex, southwestern Cyprus. *Sed. Geol.*, **98**, 245–262.

Stow, D.A.V., **Faugères, J.-C.** and **Gonthier, E.** (1986) Facies distribution and textural variation in Faro Drift contourites: Velocity fluctuation and drift growth. *Mar. Geol.*, **72**, 71–100.

Stow, D.A.V., **Faugères, J.-C.**, **Viana, A.R.** and **Gonthier, E.** (1998) Fossil contourites: a critical review. *Sed. Geol.*, **115**, 3–31.

Stow, D.A.V., **Hernández-Molina, F.J.**, **Llave, E.**, **Bruno, M.**, **García, M.**, **Díaz del Río, V.**, **Somoza, L.** and **Brackenridge, R.E.** (2013) The Cadiz Contourite Channel: sandy contourites, bedforms and dynamic current interaction. *Mar. Geol.*, **343**, 99–114.

Stow, D.A.V., **Hernández-Molina, F.J.**, **Llave, E.**, **Sayago-Gil, M.**, **Díaz-del Río, V.** and **Branson, A.** (2009) Bedform-velocity matrix: the estimation of bottom current velocity from bedform observations. *Geology*, **37**, 327–330.

Stow, D.A.V., **Hunter, S.**, **Wilkinson, D.** and **Hernández-Molina, F.J.** (2008) The nature of contourite deposition. In: *Contourites* (Eds Rebesco, M. and Camerlenghi, A.), *Dev. Sedimentol.*, **60**, 143–156.

Stow, D.A.V., **Kahler, G.** and **Reeder, M.** (2002) Fossil contourites: Type example from an Oligocene palaeoslope system, Cyprus. In: *Deep-Water Contourite Systems: Modern Drifts and Ancient Series, Seismic and Sedimentary Characteristics* (Eds Stow, D., Pudsey, C., Howe, J., Faugères, J.-C. and Viana, A.), *Geol. Soc. London Mem.*, **22**, 443–455.

Tateo, F., **Morandi, N.**, **Nicolai, A.**, **Ripepe, M.**, **Coccioni, R.**, **Galeotti, S.** and **Baudin, F.** (2000) Orbital control on pelagic clay sedimentology: the case of the late Albian "Amadeus Segment" (central Italy). *Bull. Soc. Geol. Fr.*, **171**, 217–228.

Uchman, A. and **Wetzel, A.** (2011) Deep-sea ichnology: The relationships between depositional environment and endobenthic organisms. In: *Deep-Sea Sediments* (Eds Hüneke, H. and Mulder, T.), *Dev. Sedimentol.*, **63**, 517–556.

Viana, A.R. (2008) Economic relevance of contourites. In: *Contourites* (Eds Rebesco, M. and Camerlenghi, A.), *Dev. Sedimentol.*, **60**, 493–510.

Viana, A.R., **Almeida Jr., W.**, **Nunes, M.C.V.** and **Bulhões, E.M.** (2007) The economic importance of contourites. In: *Economic and Palaeoceanographic Significance of Contourite Deposits* (Eds Viana, A.R. and Rebesco, M.), *Geol. Soc. London Spec. Publ.*, **276**, 1–24.

von der Heydt, A. and **Dijkstra, H.A.** (2006) Effect of ocean gateways on the global ocean circulation in the late Oligocene and early Miocene. *Paleoceanography*, **21**, PA1011.

Wetzel, A., **Werner, F.** and **Stow, D.A.V.** (2008) Bioturbation and biogenic sedimentary structures in contourites. In: *Contourites* (Eds Rebesco, M. and Camerlenghi, A.), *Dev. Sedimentol.*, **60**, 183–202.

Winterwerp, J.C. and **Van Kesteren, W.G.M.** (2004) *Introduction to the Physics of Cohesive Sediment in the Marine Environment. Dev. Sedimentol.*, **57**, Elsevier, Amsterdam, 466 pp.

Manuscript received 10 March 2020; revision accepted 6 August 2020